UNIVERSIDADE
BEIRA INTERIOR

Avaliação do Desempenho de Conversores DC-DC Baseados em Semicondutores de Última Geração Aplicados a Sistemas de Iluminação LED

João Paulo Marcelino Dinis

Dissertação para obtenção do Grau de Mestre em
Engenharia Eletrotécnica e de Computadores
(2º ciclo de estudos)

Orientador: Prof. Doutor António João Marques Cardoso

junho de 2020

EMPTY PAGE

UNIVERSIDADE
BEIRA INTERIOR

Performance Evaluation of DC-DC Converters Based on Last-Generation Semiconductors for LED Lighting Systems

João Paulo Marcelino Dinis

Dissertation for obtaining the degree of Master of Science in
Electrical and Computer Engineering
(2nd cycle of studies)

Supervisor: Prof. Dr. António João Marques Cardoso

June of 2020

EMPTY PAGE

Acknowledgments

I dedicate this work to my family, specially my parents for all the support they gave me and for all the effort they made thought out these years, for all the things they abdicated in order to making it possible for me to reach this step in my life and to my aunt for all the concerned calls, support and encouragement.

To my master dissertation adviser Prof. Dr. António João Marques Cardoso, a word of appreciation and gratitude for giving me the privilege to perform my work at CISE-Electromechatronic Systems Research Centre surrounded by excellent researchers and for having the opportunity to use state of the art equipment and be presented with excellent and innovative projects and research.

To Fernando Bento, I show my gratitude for all the technical advices and all the documentation, for all the support and for all the hours spent helping me.

Finally to the colleagues and friends I have made in UBI, to Ricardo, Hugo and Henrique for all their help, for all their advices and for all the fun and stress relieving moments and for all the beer and the best years of my life, and to Marcelo for all the support and friendship in these last difficult months.

EMPTY PAGE

Resumo

Os semicondutores de banda-proibida larga ou semicondutores *wide bandgap* (WBGS) são vistos como o próximo passo evolutivo na engenharia eletrónica. Esta tecnologia de semicondutores, relativamente recente, tem grandes vantagens quando comparada com tecnologias tradicionais, baseadas em semicondutores de silício (SiS). Os WBGS podem operar a frequências de comutação muito superiores, permitem uma maior tensão dreno-fonte e toleram temperaturas de funcionamento mais elevadas. Todos estes fatores resultam num rendimento operacional superior ao observado em sistemas equivalentes baseados em SiS, bem como na possibilidade de projetar e construir sistemas mais compactos, consequência especialmente atrativa para uso em veículos elétricos e híbridos, conversores de potência e outras aplicações de alta potência. Combinada com as preocupações ambientais e de mudanças climáticas, a necessidade de projetar sistemas de conversão de energia cada vez mais eficientes conduziu a um aumento dos esforços de investigação sobre o uso de WBGS em conversores de energia. Quando combinados com luminárias LED de alto rendimento, os controladores de LEDs baseados em WBGS podem representar poupanças significativas nos consumos de energia em aplicações como a iluminação em residências, grandes escritórios, edifícios públicos, ruas, etc.

Para melhor compreender as vantagens da aplicação de WBGS em conversores eletrónicos de potência, aplicados a sistemas de iluminação LED, este trabalho estabelece uma análise comparativa do desempenho de dois conversores electrónicos de potência idênticos, sendo um deles baseado em WBGS e outro baseado em SiS.

Palavras-chave

Conversores DC-DC; Dispositivos de banda-proibida larga; sistemas de iluminação LED.

EMPTY PAGE

Abstract

Wide bandgap semiconductors (WBGS) are seen as the next evolution in the field of power electronics. This relatively recent semiconductors technology shows great advantages when compared with the traditional technology, based on silicon semiconductors (SiS). WBGS are able to operate at much higher switching frequencies, allow higher gate-source voltage, and tolerate higher temperatures. Altogether, these factors lead to much higher energy conversion efficiency, when compared to equivalent Si-based power conversion systems, and enable the possibility to design and build more compact systems, especially attractive for use in electric and hybrid vehicles, power converters and other high-power applications. Combined with environmental and climate change concerns, the compelling need to design more efficient power conversion systems promoted the research on the use of WBGS in power converters. When paired with high efficiency LED fixtures, WBG-based LED drivers can bring significant savings in terms of power consumption made at homes, large offices, public buildings, streets, and so on.

To better assess the advantages of the utilisation of WBGS in power electronic converters, applied to LED lighting systems, this thesis establishes a comparative analysis of the performance of two similar power electronic converters: the first converter resorts to WBGS, while the second converter adopts SiS as the switching devices.

Keywords

DC-DC converters; wide bandgap semiconductor devices; LED lighting systems.

EMPTY PAGE

Index

List of Figures

List of Tables

EMPTY PAGE

List of Acronyms

DC - Direct Current

AC - Alternate Current

CCM - Continuous Conduction Mode

DCM - Discontinuous Conduction Mode

GaN - Gallium Nitrite

HVDC – High-Voltage Direct Current

LED – Light-Emitting Diode

MOSFET - Metal Oxide Semiconductor Field-Effect Transistor

PWM - Pulse Width Modulation

$R_{ds_{on}}$ - Drain to Source ON State Resistance for the Given V_{gs}

RGB - Red, Green, Blue

SiC - Silicon Carbide

SiS - Silicon Semiconductor

V_{gs} - Gate to Source Voltage

WBGS - Wide Bandgap Semiconductor

EMPTY PAGE

Chapter 1

Introduction

In a world facing an ever-increasing dependency on electronic and electric equipment, extensive to all sectors of activity - from industry to transportation and to domestic sectors, the total electric energy consumption keeps following a steady increment, year after year. In 2018, the global energy consumption reached 23 PWh. Estimates indicate this indicator will tend to increase even more, particularly thanks to the adoption of electric and hybrid vehicles and to the increment of electric energy consumption in developing countries [1]. Along with the increasing electric energy consumption, environmental and economic concerns have been demanding ever-increasing energy efficiency standards, in order to comply with stringent institutional and government regulations.

One of the means to achieve such demanding energy efficiency goals is precisely the adoption of cutting-edge technologies in the field of power electronics. Power conditioning is vital in many applications and also one of the domains with higher margin for improvements in terms of efficiency. Therefore, the study and use of new semiconductor technologies, capable of achieving higher figures of merit, recently became an attractive topic of study. It is here that the use of WBGS becomes of great relevance. The ability of these devices to switch at higher frequencies and the capability of operating at higher voltages and temperatures, when compared to conventional semiconductors, translates into smaller hardware structure, and a more compact and efficient energy conversion system.

EMPTY PAGE

Chapter 2

DC energy distribution, consumption, and efficiency

2.1 Historical contextualisation

At the end of the 19th century and beginning of the 20th century, two alternative electricity distribution systems were available, using direct current (DC) and alternating current (AC). The DC system, supported by Thomas Edison, was based on a low voltage DC distribution grid. Due to the limitation of DC electricity distribution systems to low voltage levels, the high currents needed for large power installations would translate into large Joule losses, caused by the considerable resistance of the long power lines. In practice, this means that DC electricity could only be transported over short distances. For large cities or large industrial centres, several power plants would be required and installed nearby. The competing AC distribution system, supported by George Westinghouse and Nikola Tesla, consisted of the use of high-voltage distribution lines carrying AC electricity. For the same power levels, the Joule losses induced by the resistance of the power lines would be much smaller, when compared to the equivalent DC distribution system. In order to transport large amounts of power, the AC distribution system relied on a step-up transformer, in order to increase the low voltage power at the output of a power plant, to be transmitted over long distances, with lower current and, consequently, lower Joule losses. At the end of the transmission line, a step-down transformer would be used to lower the voltage to safer and usable levels. The adoption of this system meant that a smaller number of high-power, high efficiency power plants would be needed. In addition, the generated power could be transmitted with reduced losses. At the time, the only way to efficiently step-up and step-down the voltage at high power levels was using transformers, an equipment that only operates in AC. Such fact explains why electric grids grew and evolved using AC until our days.

2.2 High-Voltage Direct Current power transmission

With the uptake of power electronics, it became possible to efficiently step up and step down the voltage, either at low- or high-power levels. Many high-power DC transmission lines are already in use across the world, with many more under construction. The country taking the lead in terms of high power, distance, and number of high-voltage direct current (HVDC) power lines is currently China, with projects like the Qhundong-Wannan project. This HVDC grid reaches voltages of ±1100 kV, and can carry a total maximum power of 12 GW, over a distance of 3400 Km [2].

2.2.1 Advantages

Despite the higher costs of implementation and maintenance, HVDC power transmission presents less losses when compared to conventional AC power transmission. Losses caused by the skin effect and the charging and discharging of the cables' parasitic inductance and capacitance, on every power cycle, can be quite significant, especially in underground and underwater environments, where the capacitance formed between the power lines and the surroundings can be extremely high and hard to mitigate. In HVDC power transmission, the losses induced by the skin effect and the cable parasitics are non-existent. This means that, for the same power level, cabling is smaller in diameter, on the one hand, and that the losses in transmission are smaller, on the other hand. HVDC power transmission also becomes an attractive solution to establish the connection between unsynchronised AC power grids or power grids with different frequencies.

2.2.2 Disadvantages

The most significant disadvantage of HVDC power transmission is still the cost involved in the installation and maintenance of the complex equipment required to establish HVDC grids. On the other hand, the reliability of the systems and the losses involved in the conversion of AC to DC and back to AC are additional concerns. These conversion losses can often be larger than the losses in transmission over short distances. Also, the DC current is more difficult to switch off due to the absence of zero crossing of the current [3].

2.3 DC energy consumption

Nowadays, almost every household appliance runs on DC, and most of the appliances that run on AC can also run on DC. From LED-based illumination to inverter-based air conditioners and refrigerators, as well as direct-drive washing machines and electronic appliances, like TV's, computers, smartphone chargers, and others, are all examples of DC-compatible appliances. In order to convert the AC, provided by the distribution grid, to DC, it is necessary to use a rectifying circuit, which has energy losses intrinsic to its construction.

The complexity of rectifying circuits may vary, depending on the output power level or the type of load to which they are targeted. Currently, every single appliance that runs on DC has some sort of highly inefficient rectifying circuit. The energy consumption associated to DC-compatible appliances represents the majority of the overall energy consumption of an average house in the European Union. Figure 1 shows the final energy consumption in the residential sector, by end-use, in the European Union [4].

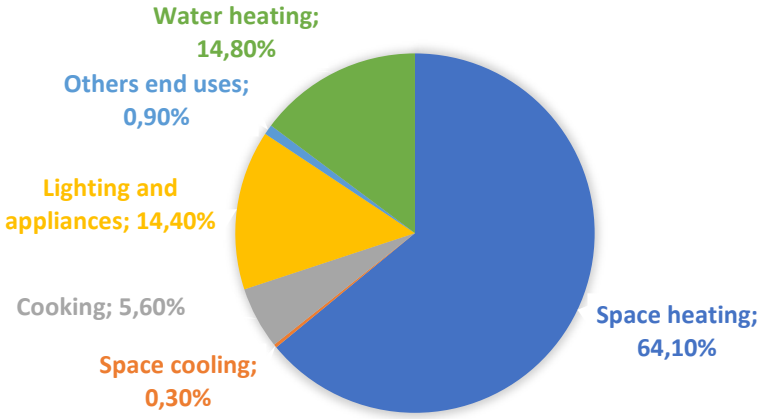

Figure 1: Final energy consumption in the residential sector, by end-use.

The previous statement means that the power losses taking place due to energy conversion processes and the costs associated with the extra components are multiplied by the number of appliances that run on DC. It is, therefore, beneficial to consider an alternative solution, consisting of a single rectifier, that converts the AC coming from the grid to DC, and distributes the DC energy throughout the entire house. Such alternative concept results in more cost-effective appliances and a more efficient use of energy. Research indicates that the energy losses of a home using DC could be reduced by around 15% when compared to an equivalent AC-supplied home [5]. In addition to the aforementioned advantages, the implementation of microgeneration

and energy storage systems also benefits from the adoption of DC-based energy distribution systems. Considering that energy is stored in batteries in the form of DC energy, and that the great majority of microgeneration systems are based on solar panels that produce DC energy, the whole architecture and interconnections between generation, consumption, and grid can be made in a simpler and effective manner when considering DC electricity distribution. One example of this statement can be found in [6].

Chapter 3

DC-DC converters

Nowadays, the majority of the low- and medium-power electric devices, particularly those used at homes, and offices, run on DC. These devices have a huge range of nominal input voltages, and many times have different voltage rails within themselves. Electronic devices, in particular, may have rails of 48V, 24V, 12V, 5V, 3.3V, 1.8V, 1.2V or 0.8V. With the exception of small-power or special applications, where a linear regulator or even a resistor dropper is used for a clean, noise-free supply, DC-DC converters are the excellence device for generating these different voltage rails, thanks to their high efficiency and smaller footprint, ideal for higher power applications. These devices offer, however, a few disadvantages. The high output ripple and high EMI are both a by-product of the switching nature of these converters. Because some loads, like audio equipment, are extremely sensitive to high voltage or current ripple, attention must be paid to the filtering of the input and output of the DC-DC converter.

Since the emergence of power electronics, and with the establishment of a wider offer of power MOSFET, in the 1970s [7], DC-DC converters have been in constant development and improvement. These converters have seen a great reduction in size and also a great increment of efficiency, thanks to the improvements attained in the MOSFET' technology. Smaller footprint, smaller $R_{ds_{on}}$, and reduced parasitic capacitances and inductances were the most remarkable advances in the technology. As a result, state-of-the-art DC-DC converters feature higher switching frequencies, higher power, smaller heatsinks and, consequently, smaller physical dimensions.

3.1. Typical Topologies

DC-DC converters can be divided into three basic categories, depending on the difference between the input and the output voltages. If the converter is used to raise the input voltage, the converter is defined as a boost converter. In turn, a buck converter is used to lower the input voltage. If the converter has the ability to either

step up or step down the input voltage, it is called a boost-buck converter. For all the three categories, there are multiple topologies deriving from the basic converter configurations. The practical interest of each topology depends on the target application and rated power of the converter. The following sub-section presents the typical circuit configurations and the working principles of the most relevant DC-DC converter topologies, with potential for LED lighting applications.

3.1.1 Boost Converter

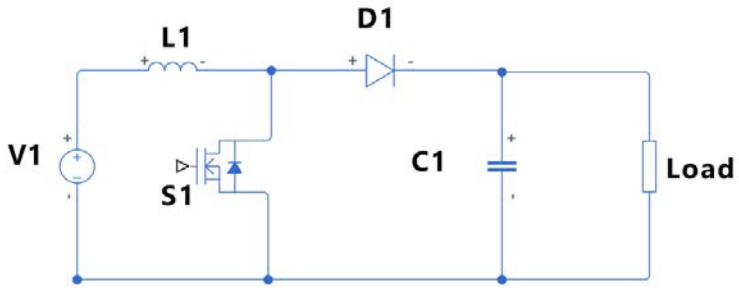

Figure 2: Typical boost converter topology.

Figure 2 represents a typical asynchronous boost converter, used to raise the voltage at the output. This topology consists of an inductor, a diode (generally a Schottky diode), a switching device, and an output filtering capacitor. This topology is one of the simplest and most reliable topologies of a boost converter, because of its reduced number of components and ease of control.

This boost converter has the following working principle:

- From t_0 to t_1, the switch S1 is turned on. The source is effectively short-circuited through inductor L1. This current creates a magnetic field in inductor L1. During this period, diode D1 is reverse-biased, which means that no current

will flow through it. At the same time, capacitor C1 provides current to the load, in accordance with Figure 3.

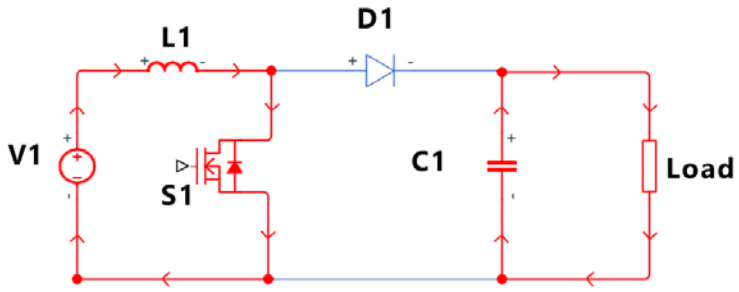

Figure 3: Boost converter current flow for the period $t_0<t<t_1$.

- From t_1 to t_2, switch S2 is turned off. The magnetic field inside L1 collapses, creating an electromotive force, according to Faraday's law, thus establishing a positive potential differential across the terminals of the inductor. D1 is now forward-biased and starts conducting current to the load and to the capacitor C1, charging it, as represented on Figure 4.

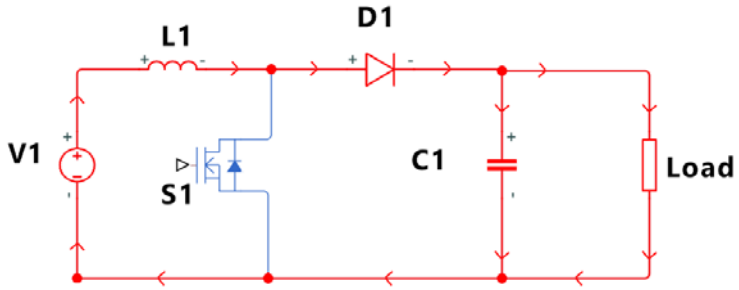

Figure 4: Boost converter current flow for the period $t_1<t<t_2$.

- From t_2 to t_3, the magnetic field in L1 collapses completely. Therefore, the potential differential across the terminals of the inductor is zero. The diode D1 is reverse-biased again, while capacitor C1 provides current to the load, according to Figure 5. This period only occurs in case that the converter operates in discontinuous conduction mode (DCM).

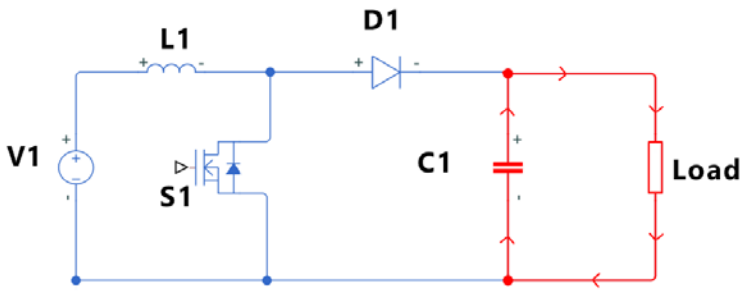

Figure 5: Boost converter current flow for the period $t_2<t<t_3$.

3.1.2 Buck Converter

Figure 6 represents a typical asynchronous buck converter, used to generate an output voltage lower than the input voltage. Like the boost converter, the buck converter is based on a switching device, an inductor, a diode, and an output filtering capacitor. As the switching device is connected at the high-side, the driving method becomes more challenging. If the device is of NPN type, it is required to generate a gate voltage higher than the source voltage V1. Generally, a boot-strap circuit is used to generate a voltage higher than the drain voltage. One alternative solution consists of using a PNP device. Unfortunately, PNP devices tend not to be used because of their lower efficiency.

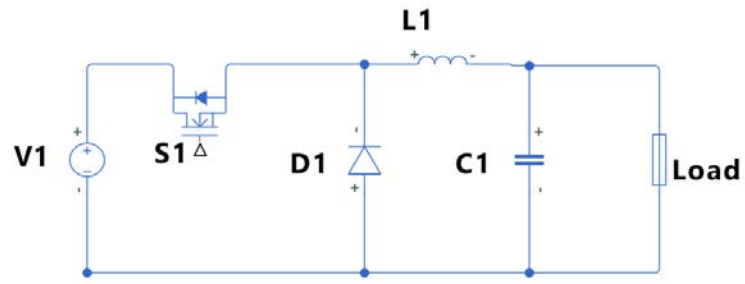

Figure 6: Buck converter topology.

This buck converter has the following working principle:

- From t_0 to t_1, the switch S1 in turned on, allowing the source current to flow through the inductor L1 and the load, as represented in Figure 7. Capacitor C1 is also charged during this period. The diode D1 is reversed-biased. A magnetic field is created in L1.

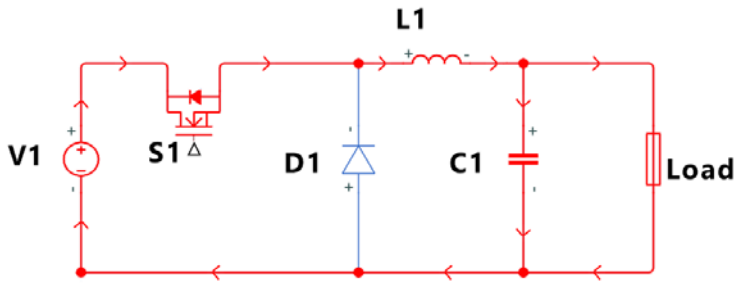

Figure 7: Buck converter current flow for the period $t_0<t<t_1$.

- From t_1 to t_2, the switch S1 is turned off. The magnetic field in L1 collapses, creating a negative voltage between D1 and L1 which, in turn, allows current to flow through D1, that is now forward-biased. This current also flows through the load and the capacitor C1, as represented in Figure 8.

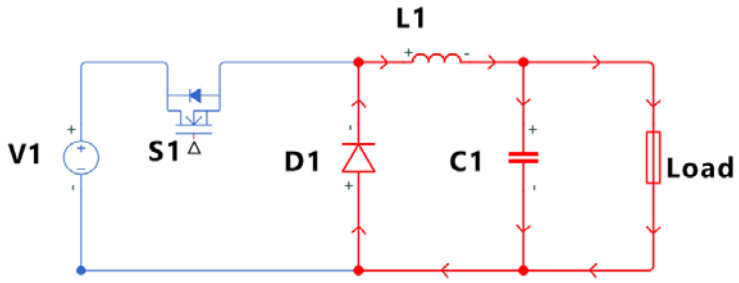

Figure 8: Buck converter current flow for the period $t_1<t<t_2$.

- From t_2 to t_3, the diode D1 is reverse-biased. No current flows through the diode D1 neither the inductor L1. During this period, capacitor C1 provides current to

the load, as represented on Figure 9. This period only occurs in case that the converter operates in DCM.

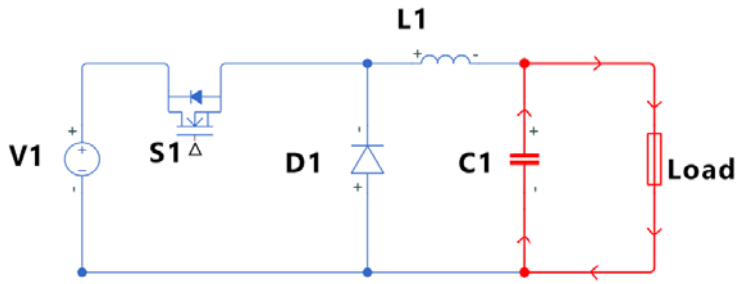

Figure 9: Buck converter current flow for the period $t_2<t<t_3$.

3.1.3 Boost-buck converter

As the name itself suggests, the boost-buck converter is a device capable of generating either a higher or lower output voltage. Figure 10 represents a typical configuration of a four-quadrant boost-buck circuit, based on four switches and an inductor. This device is also bi-directional, meaning that it can transfer energy from the source to the load, as well as from the load to the source.

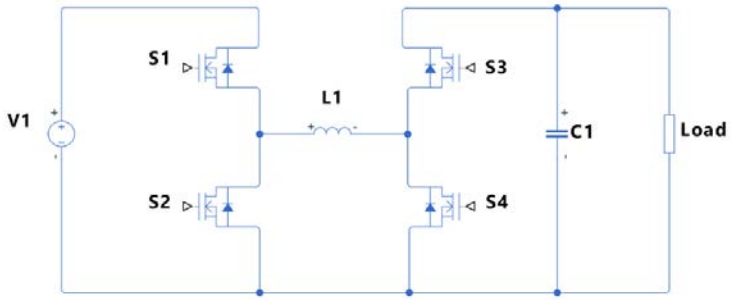

Figure 10: Boost-buck converter topology.

3.1.3.1 Boost-buck converter in buck operation mode

The operation of the boost-buck converter in buck mode is guided by the following working principles:

- From t_0 to t_1, the switches S1 and S3 are turned on, while switches S2 and S4 are turned off. Current flows through inductor L1, charging the capacitor C1 and feeding the load. This is represented in Figure 11.

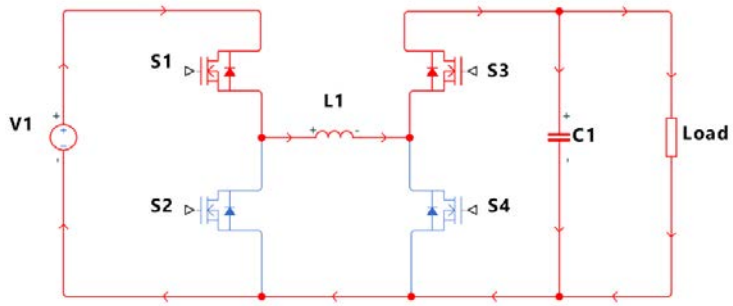

Figure 11: Current flow, in buck operation mode, for the period $t_0<t<t_1$.

- From t_1 to t_2, the switch S1 is turned off, while switch S2 is turned on, to provide a path to sustain the current flow in the load, as shown in Figure 12.

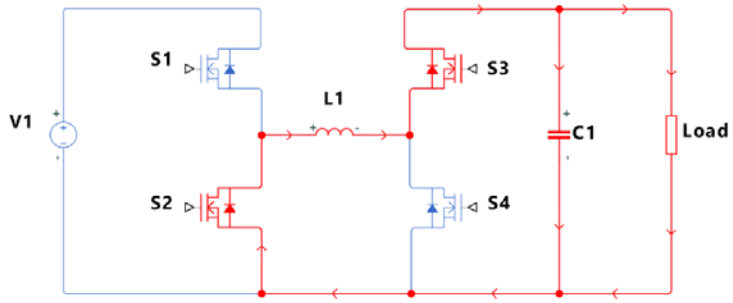

Figure 12: Current flow, in buck operation mode, for the period $t_1<t<t_2$.

- From t_2 to t_3, all switches are turned off. Capacitor C1 provides energy to the load, as shown in Figure 13. This period is solely verified in case that the converter operates in DCM.

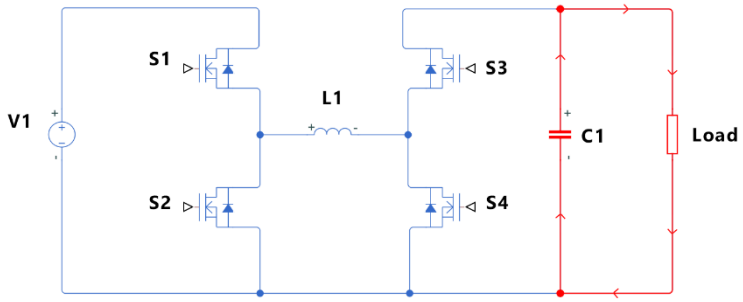

Figure 13: Current flow, in buck operation mode, for the period $t_2<t<t_3$.

3.1.3.2 Boost-buck converter in boost operation mode

The operation of the boost-buck converter in boost mode is guided by the following working principles:

- From t_0 to t_1, switches S1 and S4 are turned on, allowing current to flow through inductor L1, thus creating a magnetic field. During this period, the capacitor C1 will provide current to the load, according to Figure 14.

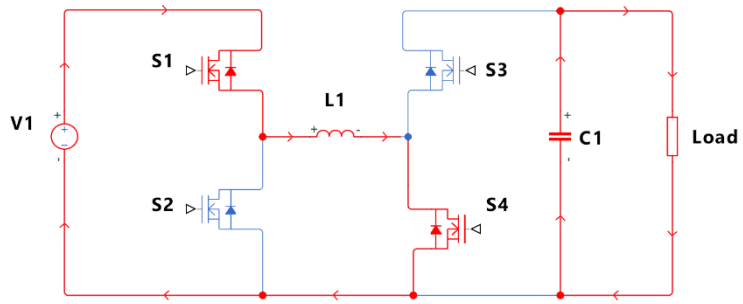

Figure 14: Current flow, in boost operation mode, for the period $t_0<t<t_1$.

- From t_1 to t_2, switch S4 is turned off, while switch S3 is turned on. As the magnetic field inside L1 collapses, an electromotive force is established according to Faraday's law, meaning that a positive potential differential will appear across the terminals of the inductor. Current will now flow to both the capacitor C1 and the load, according to Figure 15.

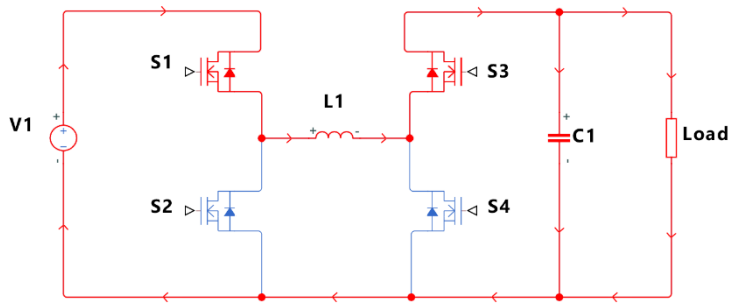

Figure 15: Current flow, in boost operation mode, for the period $t_1<t<t_2$.

- From t_2 to t_3, all the switches are turned off, allowing capacitor C1 to discharge through the load, according to Figure 16. This period of operation is solely valid for DCM operation.

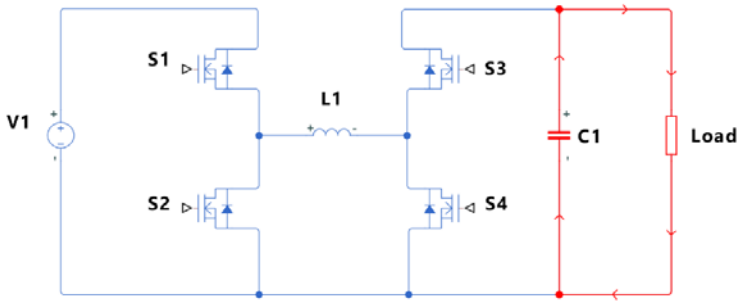

Figure 16: Current flow, in boost operation mode, for the period $t_2<t<t_3$.

This configuration of the boost-buck converter also allows the bidirectional flow of current, depending on the commutation order of the switching devices. Converters based on this topology are especially useful for applications where an electromotive force is developed at the load and the source has the ability to receive this energy.

EMPTY PAGE

Chapter 4

LED lighting systems

4.1 LED efficiency

In recent years, there has been a significant adoption of LED lighting technologies, in almost every application where light is required, ranging from residential lighting to public illumination and to automotive applications. Due to their higher brightness, higher efficiency, longer lifetime, lower profile, and the ever-decreasing production costs, LEDs are now the trending lighting technology, having replaced traditional incandescent and halogen lightbulbs. The uptake of LED lighting is being boosted by governments' policies and institutional regulations, as well as by the increasing concerns regarding energy efficiency and the environmental impact. For the same luminous flux, LEDs can represent between 25 % and 80 % of energy savings, and last for 3 to 25 times more than a conventional incandescent light bulb. For example, when compared to an incandescent lightbulb of 60 W, a 12 W LED light is able to output roughly the same amount of light and lasts 25 times more [8]. Also, LEDs waste less energy in the form of heat, thus enabling a longer lifetime. Unfortunately, LEDs also have an important drawback. Since LEDs consist of a semiconductor device, its maximum tolerable temperature is low, when compared to an equivalent incandescent lightbulb. In practice, such statement means that there are few applications where LEDs are not a feasible technology. The standard maximum tolerable temperature for an LED is around 120 degrees Celsius [9].

4.2 LED flickering and dimming

One of the problems of LED lighting systems is flickering, usually associated with poorly designed or cheaper driver systems. Flickering often arises as the result of the application of drivers with single-wave rectification and/or unfiltered output. Flickering can be visible to humans if the percent flicker is greater than 30 %, within the [100 120] Hz frequency range [10]. When resorting to switched-mode power

converters as LED drivers, one of the strategies suitable to reduce the flickering consists of adopting high switching frequencies.

LED flickering can also be noticed when low-frequency PWM is used for dimming the brightness of the light. Dimming refers to the technique of pulsating the current between zero and a specific, constant value, aiming to achieve the intended brightness for the LED. The brightness of the light is a result of the average current flowing thought the LED, whose value is directly dependent on the duty cycle of dimmed current. In case that dimming is considered, it is equally advantageous to opt by a higher dimming frequency.

Another approach suitable to achieve brightness control consists of linear dimming, attainable by means of a setting a constant current. The brightness of the light is changed by carefully controlling the instantaneous value of the current provided to the LED. Linear dimming is advantageous when compared to PWM dimming in applications where the LED is placed far from the driver. When PWM dimming is selected, parasitic inductances and capacitances of the cabling distort and decrease the average current and result on a significant mismatch between the set and actual value of the average current.

4.3 RGB LED and light colour/temperature

Recent research on the influence of different light colours, commonly referred to as light temperature, has proven that humans are not only more sensitive to specific components of the visible spectrum, but also that these spectrum components have different impacts on the human health and well-being. The most common example of application of this statement consists of the use of a “blue filter” on displays of computers and smartphones. This filter simply applies a reduction on the intensity of the light in the blue component of the visible light spectrum, which is associated with the stimulus of the brain. Other example of the effects of distinctive colour temperatures is the illumination of different rooms in houses. Typically, bedrooms have a light source with a hotter colour, i.e. a colour closer to yellow and red, colours associated with a more comfortable and relaxing environment. In contrast, the living rooms and kitchen tend to have a colder light source, closer to blue, creating a more awakening sensation [11].

The benefits of changing the colour temperature based on the environment, the period of the day, the season of the year, and the purpose of the room or space that is being illuminated, has leveraged the interest on the adopting of RGB lighting systems that, due to the need for a more expensive and complex control system when compared to a typical fixed colour light system, have previously been relegated to small applications, like screens, projectors, and other devices used for the reproduction of images. By combining the red, green and blue lights, it is possible to create any colour of the visible spectrum as a function of the intensity percentage of each of the three colours, as shown on Figure 17.

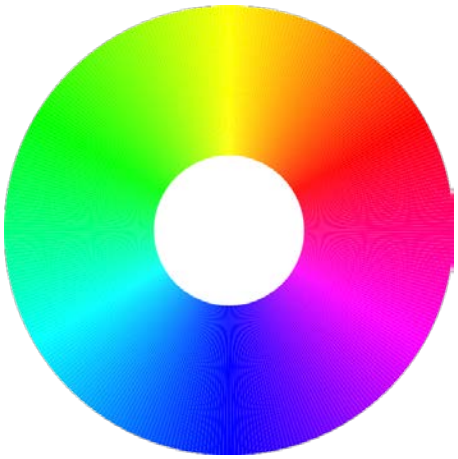

Figure 17: RGB colour wheel with 360 colours. Adapted from [12].

EMPTY PAGE

Chapter 5

Wide bandgap semiconductors

5.1 Comparation between wide bandgap semiconductors (WBGS) and silicon semiconductors (SiS)

The distinction between a conductor and an isolator can be made on a band gap basis. While an isolator typically has a band gap higher than 4 eV, a conductor material has a band gap of almost zero. Between these two materials, there are the semiconductors, materials that have properties of both isolators and conductors. That is where we find the SiS, the basis of modern electronic. While the traditional components, made of Si, have a band gap between [1 1,5] eV, the WBGS have a band gap within the range [2 4] eV. Gallium nitrite (GaN) and silicon carbide (SiC) materials appear as the most promising wide bandgap materials. The semiconductor with the widest bandgap, highest thermal conductivity and highest breakdown voltage is diamond. In the simulations and experimental tests performed for this thesis, only GaN MOSFETs will be approached. Table 1 represents some of the important parameters for GaN, Si, SiC and diamond materials.

Table 1: Some semiconductors' parameters at 300 K

Semiconductor material	**Bandgap [eV]**	**Breakdown field E_c [10^6V/cm]**	**Thermal conductivity σ_T [W/cm]**	**Coefficient of thermal expansion [ppm/K]**
Si	1,12 [13]	0.3 [14]	1,5 [14]	2,5 – 4,2 [15]
GaN	3,44 [13]	>5 [14]	1.5 [14]	3,2 -5,6 [15]
SiC	2,36 [13]	4,0 [14]	5 [14]	4,0 – 5,8 [15]
C (diamond)	5,46 - 5,6 [13]	5,7 [13]	6 - 20 [13]	1,0 – 3,8 [15]

5.2 Advantages and disadvantages

5.2.1 Advantages

As a result of the larger bandgap, WBGS can operate at higher voltage levels, with typical breakdown voltages in the order of 15 kV [16], much higher than the typical SiS breakdown voltages, located between 4,5 kV and 6,5 kV [17]. In addition to the ability of operating at higher voltage levels, WBGS are capable of operating at higher switching frequencies than the typical switching frequencies used on SiS, while keeping a high drain-source rupture voltage [18], as well as to operate at power levels of tens of kilowatts. Such features are attainable thanks to the small total gate charge (Q_g) inherent to the WBGS, which allows a faster charge and discharge of these capacitances, assuring that the device remains in the linear region for a short period. Also, a smaller electromagnetic interference (EMI) can be expected, due to the excellent switching and reverse recovery characteristics of WBGS.

To compare the performance of MOSFETs employing distinctive semiconductor materials, the $R_{ds_{on}}$ characteristic value, observed for a given voltage, is typically adopted as metric of choice. This is one of the most defining characteristics of WBGS, being the WBGS $R_{ds_{on}}$ value lower than the $R_{ds_{on}}$ value of traditional SiS, for a given breakdown voltage. In addition, WBGs have a higher thermal conductivity, better switching (higher dV/dt) and reverse recovery characteristics [19]. All these characteristics mean that less waste heat is produced, not only when the device is in the saturation region, but also when it is in the linear region. Therefore, a smaller heat dissipation solution is required for the application of these semiconductors, specially at high power levels, resulting in a more efficient device.

Since the thermal energy of electrons in the valence band increases with temperature, they can begin to move to the conduction band, resulting in an uncontrolled conduction, possibly leading to a thermal runaway situation. For WBGS, the temperature at which this phenomenon happens is located at around 900 ºC, far from the typical limit of 150 ºC for Si based devices [19]. Therefore, WBGS can tolerate much higher temperatures than SiS [20], without suffering permanent damages [21] or degradation on their performance, even though a more realistic maximum operating temperature is limited by the package material where the die is encapsulated [22].

Added to the fact that the thermal coefficient of expansion is better suited to today's ceramic-based packs [13], the thermo-mechanical stress of WBGS will be smaller than a comparable solution based on SiS. The operating temperature of WBGS

also has lower impact in the forward and reverse characteristics, translating into a more reliable device, for a broad temperature operating range.

5.2.2 Disadvantages

As WBGS are a relative recent semiconductor technology, there are still a few hurdles to overcome in what concerns their use, even though the recent interest for these devices has led to an increase in research and development, specially of SiC and GaN MOSFETs.

One of the greatest disadvantages of WBGS is the still very high cost of the technology [19]. The initial cost could overbalance the benefits of higher efficiency and the money saved in the long term. But with the increase in demand and subsequent increase in production, it is expected for the cost of manufacturing to go down, thus making these technologies more affordable and attractive. Another important disadvantage of WBGS is the low processing yield caused by defects, for SiC technology, and processing problems, for GaN and diamond technologies [19]. There are also the problems caused by the lack of proper high-temperature packaging techniques, that is currently limiting the maximum operating temperature of these semiconductors. Also, the higher ratio of the electron-to-hole mobility makes WBGS undesirable for use in bipolar devices [13].

5.3 Applications

Taking in consideration the ability of WBGS to operate at high voltages, high power levels, and high temperatures, WBGS are considered suitable for high power, high voltage, compact applications. Applications like battery chargers, power inverters, and power converters can benefit from the use of these switching devices, resulting in high efficiency and reduced weight, since the need for heat dissipation is minimal. On the other hand, the possibility to switch the device at higher frequencies can reduce the size of the passive components of the circuit.

Candidate applications range from electric and hybrid vehicles systems, like battery chargers, motor driver modules, and electric car charging stations, to renewable energy applications, like high-power maximum power point trackers and

bidirectional grid inverters. Figure 18 shows the frequency and power range of the different types of semiconductor technologies.

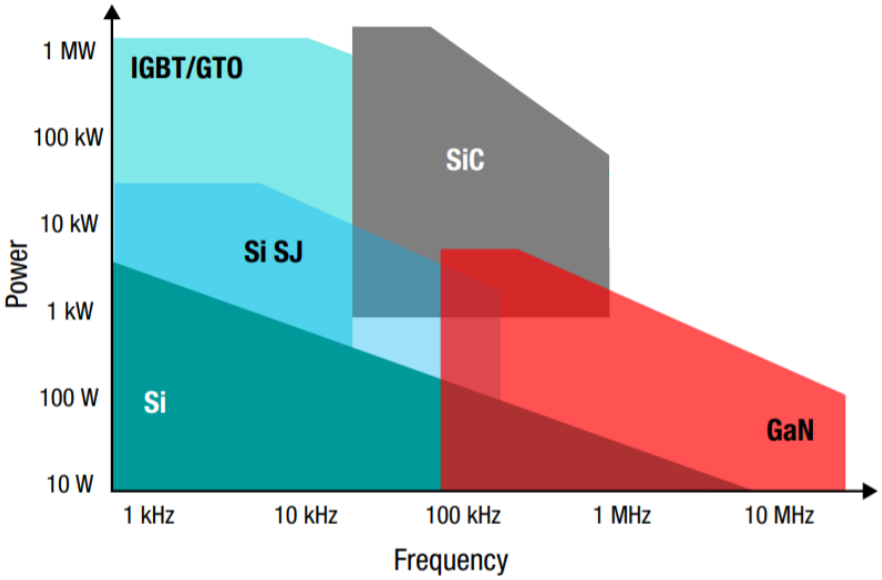

Figure 18: Power and frequency range of operation of the semiconductor technologies. Adapted from [23]

Chapter 6

Single LED, constant current synchronous buck converter

6.1 Description

In order to perform the comparison tests among the two semiconductor technologies, a simple constant current synchronous buck converter circuit was considered as the LED driver. The circuit, represented in Figure 19, is first implemented in simulation environment, using the Simulink software. This circuit was then built to be used in practical laboratory tests.

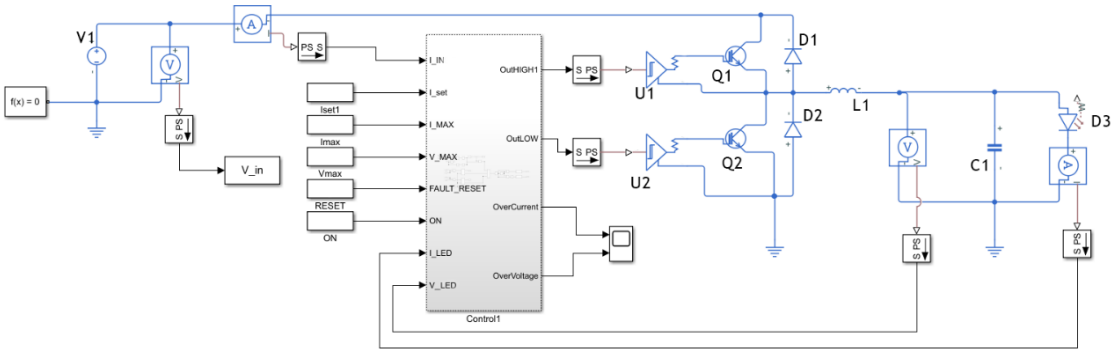

Figure 19: Representation of the synchronous buck converter considered in the study.

The circuit consists on a constant voltage source V1, an inductor L1, a capacitor C1, and two switching devices, labelled as Q1 and Q2. Both switching devices are driven by an individual gate driver, labelled as U1 and U2, controlled by the block labelled as Control1. The inductance of the driver' inductor is computed using equation 6.1, where V_{in} and V_{out} refer to the input and the output voltages, respectively, f is the main switching frequency, I_{out} is the output nominal current, and r denotes the current ripple ratio.

$$L = \frac{(V_{in} - V_{out}) \times V_{out}}{V_{in} \times f \times r \times I_{out}} \quad (6.1)$$

The value chosen for r is 0.3, meaning the maximum peak-to-peak input current ripple is equal to 30 % of the output nominal current.

To measure the input current and the current flowing through the LED, current sensors were employed. Similarly, voltage sensors were used to measure the voltage at the converter input and at the terminals of the LED. The LED device consists of a single COB LED, composed of a combination of series and parallel LED chips, with a total power of approximately 100 W and a nominal forward voltage of 32 V, at 3 A. The luminous flux is 110 lm/W and the colour temperature is specified at a warm white (between 3000 and 3200 K).

Note that the electric circuit represented as the blue lined components are part of Simscape library, while the black lined components are part of Simulink library. In order to interconnect both libraries, special blocks denoted “PS S” were employed to establish the interface among the distinctive components.

6.2 Theory of operation

6.2.1 Controller

The implemented controller, represented in Figure 20, is based on a hysteresis PWM control method with 8 bit resolution, where the control constant 0 corresponds to 0 % duty cycle and the control constant 254 corresponds to 100 % duty cycle. The controller relies on the LED current reading as the feedback signal.

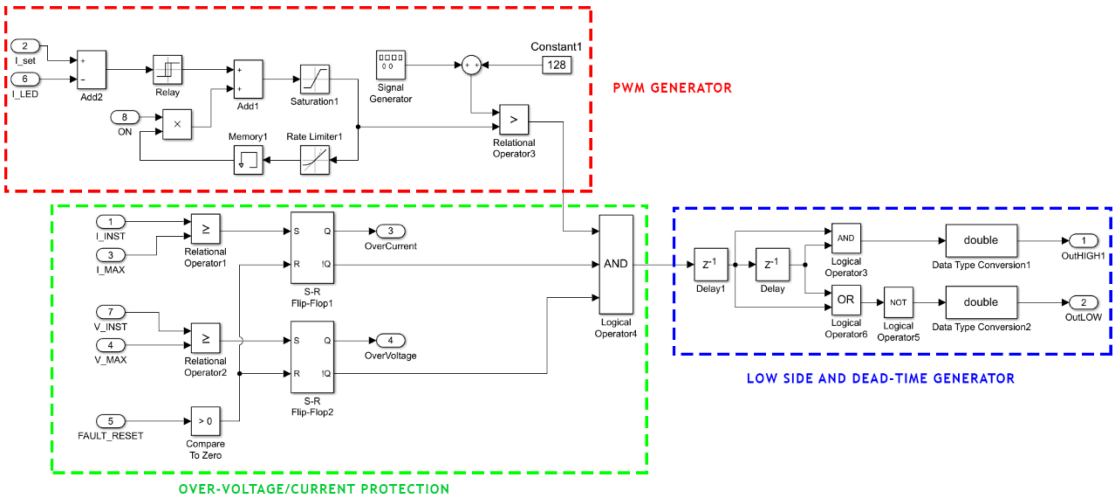

Figure 20: Controller for the single LED synchronous buck converter.

The controller is composed of a PWM generator, highlighted by the red rectangle, an over-voltage/current protection, highlighted by the green rectangle, and a low side and dead-time generator.

The PWM generator works by first calculating the error, that is, the difference between the current set value and the current read value. If the error is positive, the current read value is lower than the set value. Therefore, the controller increases the control constant by 1, which translates into an increment of the duty cycle by 2,55 %. On the other hand, if the error is negative, the current read value is higher than the set value. So, the controller decreases the control constant by 1, which translates into a decrement of the duty cycle by 2,55 %. The control constant is limited to a maximum of 242, which corresponds to approximately 95 % duty cycle. This condition is considered in order to avoid continuous conduction through the high-side switching device. Also, the rate of change of the control variable is limited, in order to avoid significant overshoots and undesired oscillations. The duty cycle value is then used to generate a PWM signal, that is fed to the over-voltage/current protection. Also, an ON/OFF command is used, to either turn ON or OFF the buck converter.

The over-voltage/current protection is used to protect the controller and LED in case of failure of any of the components of the system. If either the voltage at the LED terminals or the input current exceed the maximum established values, the controller shuts down the converter. In that case, a RESET signal must be applied in order to restart the operation of the controller.

The low side and dead-time generator is used to generate a signal to control the low side switching device and the dead time between the high-side and low-side signals, a period of time where both high- and low-side signals are at low level, as represented on Figure 21.

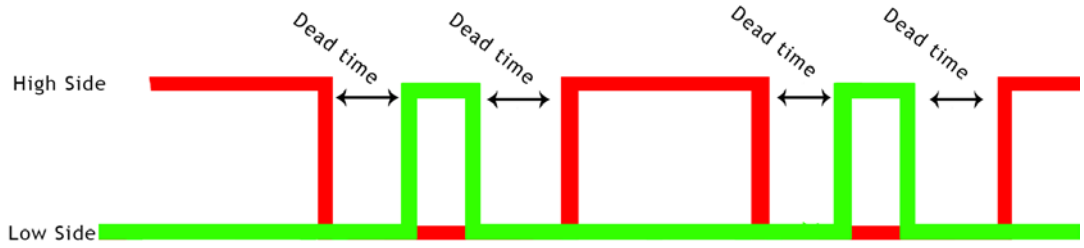

Figure 21: Dead time between high- and low-side devices.

The application of dead-time between the two gating signals is done so as to avoid shoot through, that is, to avoid having both switching devices turned on at the

same time, creating a short-circuit between the voltage source V1 and ground. The shoot through phenomenon may happen because the switching devices do not turn ON or OFF instantaneously. For the simulation, the defined dead time was the lowest time possible, meaning a 20 µs dead time.

6.3.2 Converter operation principles and power losses

The following description of the operation principles of the circuit uses a simplified schematic representation of the converter. Considering the circuit operation in steady-state mode, the current flow is as following:

- From t_0 to t_1, the switching device Q1 is turned ON and Q2 is turned OFF, allowing current to flow through the inductor L1 and the LED. During this period, the capacitor C1 is charged. This period of operation is represented in Figure 22.

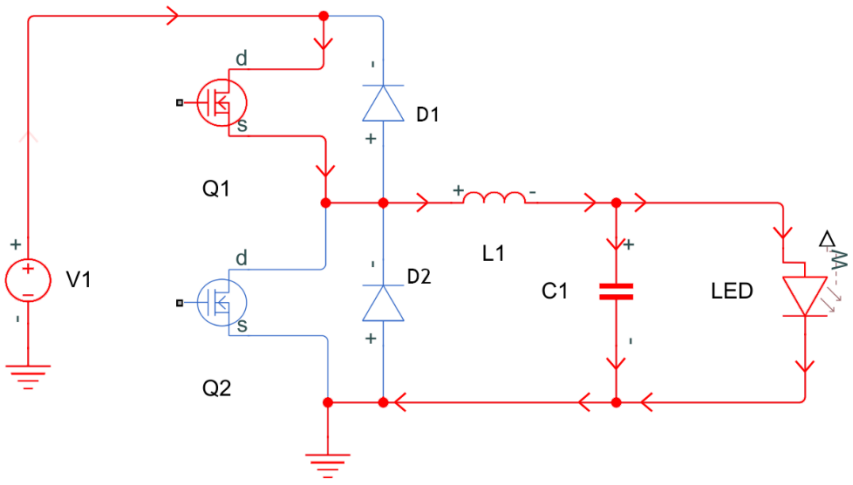

Figure 22: Current flow for the period $t_0<t<t_1$.

As current flows through L1, a magnetic field is established, opposing to the sudden changes in the current. This behaviour effectively decreases the peak current at the input.

During this period of operation, the power losses are assigned to the on-resistance of the high-side switching device, computed by equation 6.2, and the ohmic resistance of the inductor, given by the equation 6.5.

$$P_{Q\_H} = I^2_{RMS\_Q\_H} \times R_{DS(on)H} \quad (6.2)$$

where $R_{DS(on)H}$ is the on-time drain-to-source resistance of the high-side switching device, and $I^2_{RMS\_Q\_h}$ is the RMS value of the switch current, computed by equation 6.3:

$$I^2_{RMS\_Q\_H} = \frac{V_{out}}{V_{in}} \times \left(I^2_{out} + \frac{\Delta I^2}{12} \right) \quad (6.3)$$

where I_{out} denotes the output current and ΔI is the maximum current ripple. If the low impact of the current ripple on the power losses is neglected, equation 6.2 can be simplified into equation 6.4:

$$P_{Q\_H} = \frac{V_{out}}{V_{in}} \times I^2_{out} \times R_{DS(on)H} \quad (6.4)$$

The power dissipated by the inductor as a result of its ohmic resistance are computed by using equation 6.5:

$$P_L = I^2_{RMS\_L} \times R_{DCR} \quad (6.5)$$

where R_{DCR} is the inductor DC resistance and $I_{RMS\_L}{}^2$ is the inductor RMS current, given by equation 6.6:

$$I_{RMS\_L}{}^2 = I^2_{out} + \frac{\Delta I^2}{12} \quad (6.6)$$

If the low impact of the current ripple to the inductor power losses is neglected, equation 6.5 can be simplified into equation 6.7:

$$P_L = I^2_{out} \times R_{DCR} \quad (6.7)$$

- From t_1 to t_2, both Q1 and Q2 are turned OFF, to avoid shoot through. The magnetic field inside L1 collapses, creating an electromotive force which, in turn, promotes a current flow through D2, as represented in Figure 23. The capacitor C1 discharges, providing energy to the LED. Note that this period must be as short as possible.

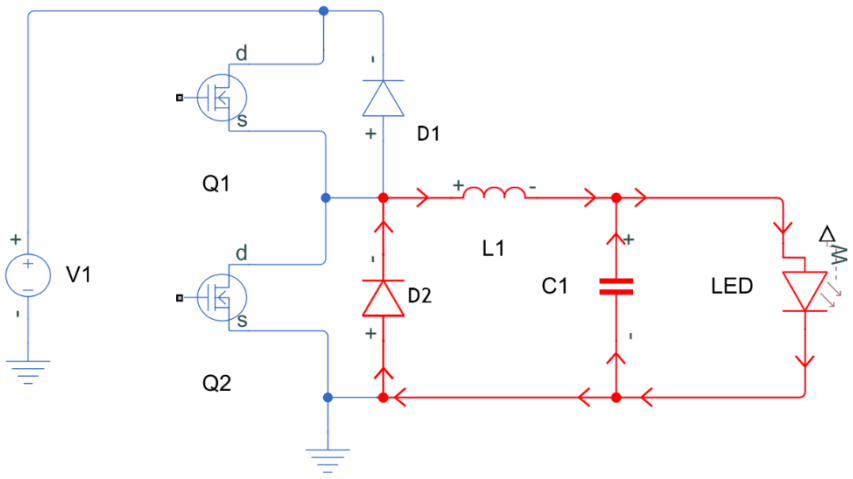

Figure 23: Current flow for the period $t_1<t<t_2$.

During this period of operation, the power dissipated in the converter is equal to the power dissipated by the inductor, given by equation 6.7, and the power dissipated by the diode, given by equation 6.8:

$$P_D = I^2_{RMS\_Q\_L} \times V_{FM} \tag{6.8}$$

where $I^2_{RMS\_Q\_l}$ is the RMS value of the diode current and V_{FM} is the diode forward voltage. Considering that this period of operation of the converter is quite short, the power dissipation taking place during this period can be neglected.

- From t_2 to t_3, switch Q2 is turned ON, so that current flows through the switch instead of the diode. Therefore, a path with lower losses is established, as shown in Figure 24. Also during this period, the capacitor keeps providing energy to the LED.

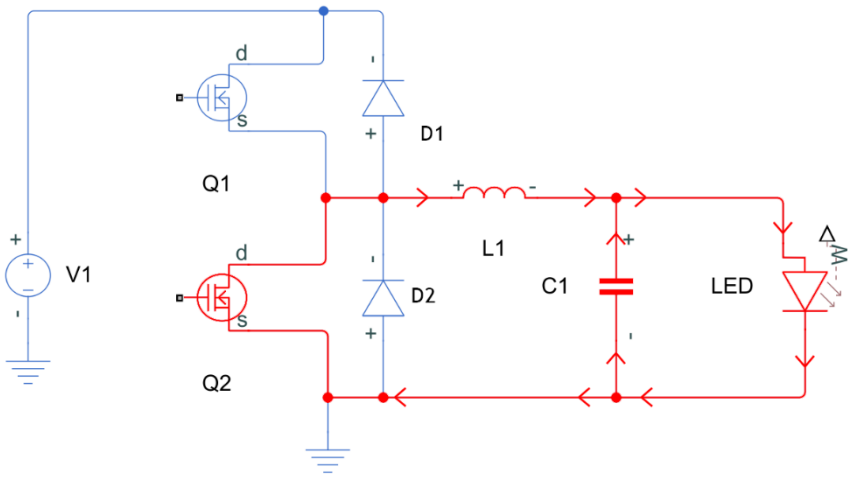

Figure 24: Current flow taking place during the period $t_2<t<t_3$.

During this period, the power dissipated in the converter can be computed as the sum of the power dissipated by the inductor and the power dissipated by the low-side switching device. The latter is given by the equation 6.9:

$$P_{Q\_L} = I^2_{RMS\_Q\_L} \times R_{DS(on)L} \tag{6.9}$$

where $I^2_{RMS\_Q\_1}$ can be computed by equation 6.10:

$$I^2_{RMS\_Q\_L} = \left(1 - \frac{V_{out}}{V_{in}}\right) \times \left(I^2_{out} + \frac{\Delta I^2}{12}\right) \tag{6.10}$$

If the value of current ripple is neglected, equation 6.9 can be re-written as equation 6.11:

$$P_{Q\_L} = \left(1 - \frac{V_{out}}{V_{in}}\right) \times I^2_{out} \times R_{DS(on)L} \tag{6.11}$$

- From t_3 to t_4, both Q1 and Q2 will be turned OFF, as shown in Figure 25, to avoid the shoot through phenomenon. This condition of operation will only be observed if the converter operates in DCM. If this current is not equal to zero, then the current flow will be as shown in Figure 22.

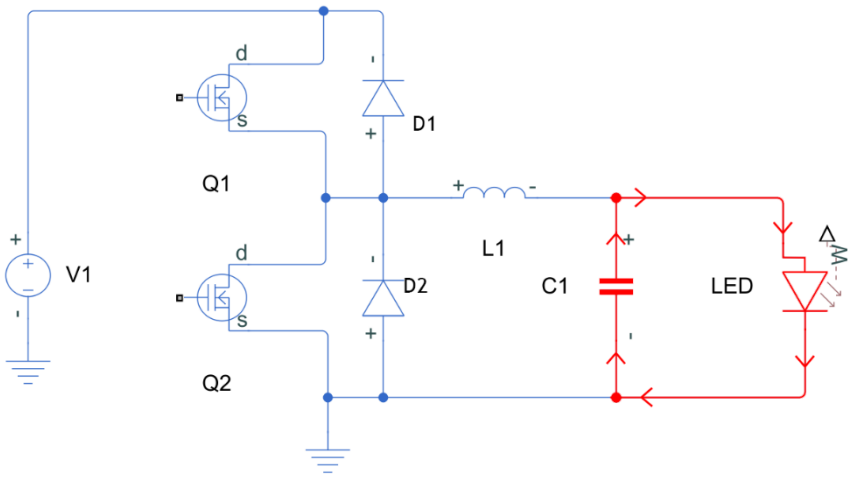

Figure 25: Current flow taking place during the period $t_3<t<t_4$.

Based on the previous analysis of the converter operation, it is possible to estimate the total power losses. Equation 6.12 can be used to express the total power dissipated in the converter:

$$P_{diss} = P_{Q\_H} + P_{Q\_L} + P_L \tag{6.12}$$

Resulting in equation 6.13:

$$P_{diss} = I_{out}^2 \times \left[\frac{V_{out}}{V_{in}} \times \left(R_{DS(on)H} - R_{DS(on)L}\right) + R_{DS(on)L}\right] \times R_{DCR} \tag{6.13}$$

Chapter 7

Simulation results

In this chapter, the simulation of the circuit will be described and the results analysed. The circuit was simulated using the software Simulink, while the software MATLAB was used to automate the process of running simulations for the distinctive values of LED current and converter switching frequency, and to retrieve and compile the data of the simulations. The simulations were run in parallel, resorting to the parallel computing toolbox, in order to speed up the simulations. Each simulation has a duration of 2 seconds and a discrete, fixed time step of 20 µs. The simulations were performed for both Si IGBTs and GaN transistors, using different PWM frequencies and output currents. The PWM frequency range from 2 kHz to 18 kHz, in 2 kHz increments. For each frequency, current values ranging from 100 mA to 3100 mA, in 200mA increments, were simulated, resulting in a total of 144 simulations for each semiconductor technology. The simulation parameters for the Si IGBTs are described in Table 2, and are based on the technical features of the SK integrated intelligent Power PACK 3-phase bridge SKiiP 132 GD power module. Meanwhile, the parameters for the GaN transistors are described in Table 3, and are based on the technical features of the GS66508B E-mode GaN transistor.

Table 2: Simulation parameters of the Si IGBTs.

Symbol	Parameter	Value	Unit
I_{ces}	Zero gate voltage collector current (V_{ce} = 1200 V)	0.4	mA
$V_{ge}(th)$	Gate-emitter threshold voltage	1.38	V
$V_{ce}(sat)$	Collector-emitter saturation voltage (I_{ce} = 125 A, V_{ge} = 2.55 V)	3.05	V
T_{amb}	Environment temperature	25	ºC
C_{ies}	Input capacitance	110.4	nF
C_{res}	Reverse transfer capacitance	2.7	nF

Table 3: Simulation parameters of the GaN transistors.

Symbol	Parameter	Value	Unit
$R_{ds(on)}$	Drain-source ON resistance (I_{ds} = 9 A, V_{gs} = 6 V)	0.05	Ω
V_{th}	Gate-source threshold voltage	1.7	V
T_{amb}	Environment temperature	25	ºC
C_{ies}	Input capacitance	260	pF
C_{rss}	Reverse transfer capacitance	65	pF

Table 4 compiles data about the performance of the buck converter in terms of efficiency, for each switching frequency and LED current level, obtained for the synchronous buck converter based on Si devices. Figure 25 depicts the data provided in Table 4, resorting to a graphical representation.

Table 4: Simulation efficiency of the buck converter based on Si devices.

I\f	2kHz	4kHz	6kHz	8kHz	10kHz	12kHz	14kHz	16kHz	18kHz
100	69,95%	67,32%	68,36%	69,41%	77,69%	72,00%	71,35%	74,13%	71,53%
300	85,77%	86,74%	87,44%	87,63%	87,16%	87,50%	87,10%	87,25%	87,19%
500	90,57%	91,22%	91,03%	90,75%	90,46%	90,88%	90,87%	91,09%	91,00%
700	92,84%	92,66%	92,48%	92,21%	92,15%	92,34%	92,38%	92,59%	92,53%
900	94,09%	93,92%	93,80%	93,67%	93,27%	93,78%	93,82%	93,95%	93,90%
1100	94,56%	94,50%	94,38%	94,35%	93,27%	94,32%	94,34%	94,51%	94,39%
1300	94,88%	94,79%	94,68%	94,67%	93,27%	94,61%	94,56%	94,78%	94,62%
1500	95,14%	95,09%	95,01%	94,97%	93,27%	94,82%	94,78%	94,94%	94,83%
1700	95,40%	95,38%	95,31%	95,29%	93,27%	94,96%	94,99%	95,11%	95,01%
1900	95,70%	95,68%	95,61%	95,58%	93,27%	95,14%	95,13%	95,27%	95,18%
2100	95,74%	95,74%	95,68%	95,64%	93,27%	95,30%	95,30%	95,41%	95,32%
2300	95,81%	95,78%	95,75%	95,70%	93,27%	95,48%	95,44%	95,53%	95,48%
2500	95,87%	95,86%	95,80%	95,79%	93,27%	95,62%	95,61%	95,66%	95,65%
2700	95,95%	95,94%	95,90%	95,86%	93,27%	95,76%	95,78%	95,77%	95,75%
2900	96,00%	95,99%	95,97%	95,89%	93,27%	95,86%	95,85%	95,87%	95,85%
3100	96,02%	95,99%	95,96%	95,91%	93,27%	95,90%	95,91%	95,92%	95,91%

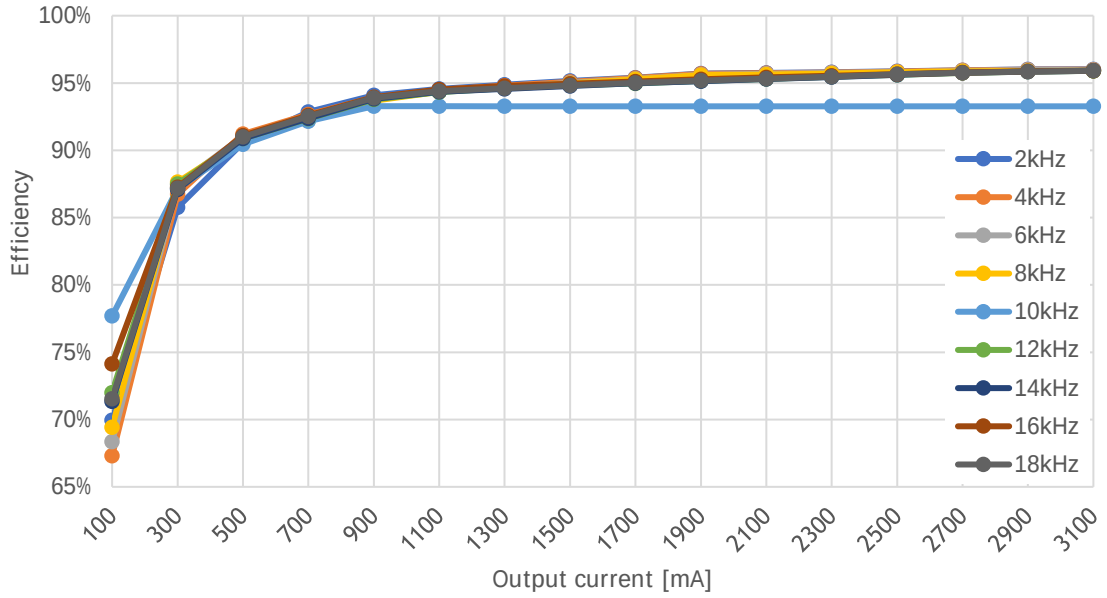

Figure 26: Simulation efficiency of the buck converter based on Si devices.

Table 5 compiles data about the performance of the buck converter in terms of efficiency, for each switching frequency and LED current level, obtained for the synchronous buck converter based on GaN devices. Figure 26 depicts the data provided in Table 5, resorting to a graphical representation.

Table 5: Simulation efficiency of the buck converter based on GaN devices.

I\f	2kHz	4kHz	6kHz	8kHz	10kHz	12kHz	14kHz	16kHz	18kHz
100	84,27%	79,84%	76,97%	74,73%	78,52%	73,61%	74,20%	76,61%	74,37%
300	90,09%	87,26%	88,74%	88,98%	90,41%	89,39%	88,82%	88,34%	88,58%
500	91,95%	92,09%	92,09%	92,11%	92,80%	92,26%	92,20%	92,24%	92,17%
700	93,59%	93,53%	93,51%	93,46%	93,83%	93,58%	93,61%	93,60%	93,62%
900	94,40%	94,45%	94,45%	94,42%	94,25%	94,57%	94,61%	94,55%	94,57%
1100	95,19%	95,24%	95,26%	95,26%	94,68%	95,21%	95,21%	95,26%	95,20%
1300	95,46%	95,47%	95,49%	95,49%	94,68%	95,36%	95,38%	95,44%	95,37%
1500	95,72%	95,71%	95,73%	95,74%	94,68%	95,49%	95,50%	95,61%	95,50%
1700	95,95%	95,98%	95,99%	95,98%	94,68%	95,62%	95,60%	95,71%	95,66%
1900	96,19%	96,21%	96,24%	96,23%	94,68%	95,78%	95,76%	95,85%	95,80%
2100	96,29%	96,32%	96,32%	96,34%	94,68%	95,92%	95,93%	95,95%	95,94%
2300	96,33%	96,34%	96,35%	96,37%	94,68%	96,06%	96,03%	96,09%	96,07%
2500	96,36%	96,38%	96,39%	96,38%	94,68%	96,21%	96,21%	96,20%	96,20%
2700	96,45%	96,45%	96,46%	96,45%	94,68%	96,36%	96,36%	96,35%	96,35%
2900	96,49%	96,50%	96,50%	96,47%	94,68%	96,41%	96,39%	96,38%	96,39%
3100	96,48%	96,50%	96,49%	96,43%	94,68%	96,43%	96,42%	96,42%	96,43%

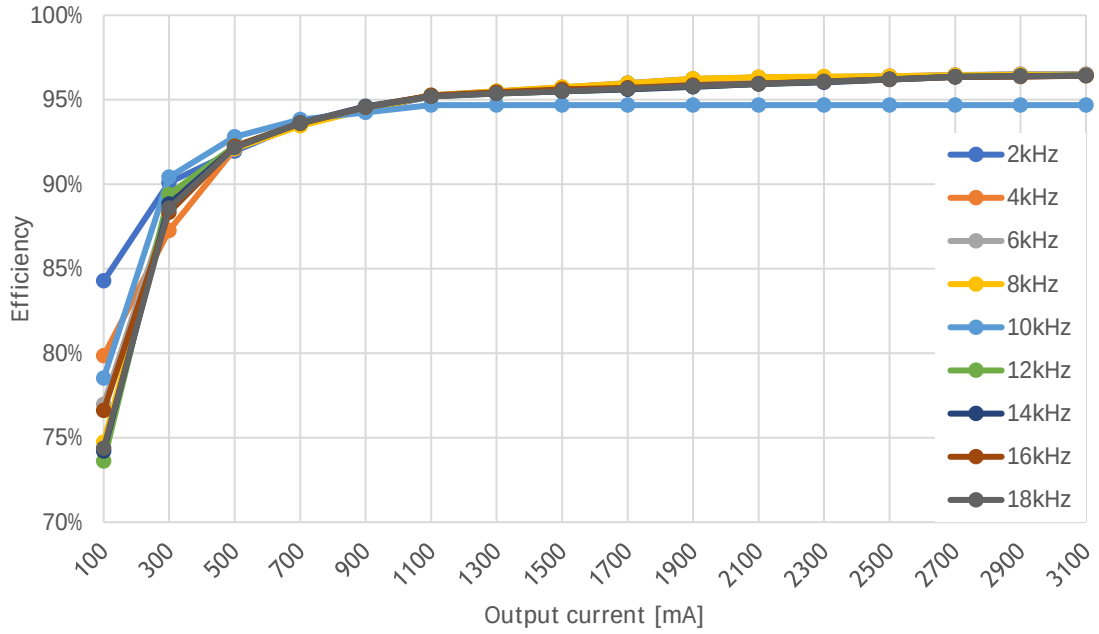

Figure 27: Simulation efficiency of the buck converter based on GaN devices.

To better evaluate the difference between the Si and the GaN technologies in terms of performance, the difference between the efficiency of both systems was computed. The results of such exercise are represented in Table 6 and Figure 27.

Table 6: GaN vs Si efficiency difference.

I\f	2kHz	4kHz	6kHz	8kHz	10kHz	12kHz	14kHz	16kHz	18kHz
100	14,33%	12,52%	8,61%	5,32%	0,83%	1,61%	2,86%	2,49%	2,84%
300	4,32%	0,51%	1,30%	1,35%	3,25%	1,89%	1,72%	1,08%	1,38%
500	1,38%	0,87%	1,06%	1,36%	2,35%	1,39%	1,32%	1,15%	1,17%
700	0,74%	0,87%	1,03%	1,25%	1,68%	1,24%	1,24%	1,00%	1,09%
900	0,32%	0,54%	0,65%	0,74%	0,98%	0,78%	0,79%	0,60%	0,67%
1100	0,63%	0,74%	0,88%	0,91%	1,42%	0,89%	0,86%	0,75%	0,80%
1300	0,58%	0,68%	0,80%	0,82%	1,42%	0,76%	0,83%	0,66%	0,76%
1500	0,57%	0,61%	0,72%	0,77%	1,42%	0,67%	0,72%	0,66%	0,67%
1700	0,56%	0,60%	0,68%	0,69%	1,42%	0,66%	0,61%	0,60%	0,64%
1900	0,49%	0,53%	0,63%	0,65%	1,42%	0,63%	0,63%	0,58%	0,62%
2100	0,55%	0,58%	0,63%	0,70%	1,42%	0,62%	0,63%	0,54%	0,62%
2300	0,52%	0,56%	0,61%	0,66%	1,42%	0,58%	0,58%	0,56%	0,59%
2500	0,50%	0,53%	0,59%	0,59%	1,42%	0,59%	0,60%	0,54%	0,55%
2700	0,49%	0,52%	0,56%	0,59%	1,42%	0,61%	0,58%	0,58%	0,60%
2900	0,48%	0,51%	0,54%	0,58%	1,42%	0,56%	0,54%	0,51%	0,55%
3100	0,46%	0,50%	0,53%	0,52%	1,42%	0,53%	0,51%	0,51%	0,52%

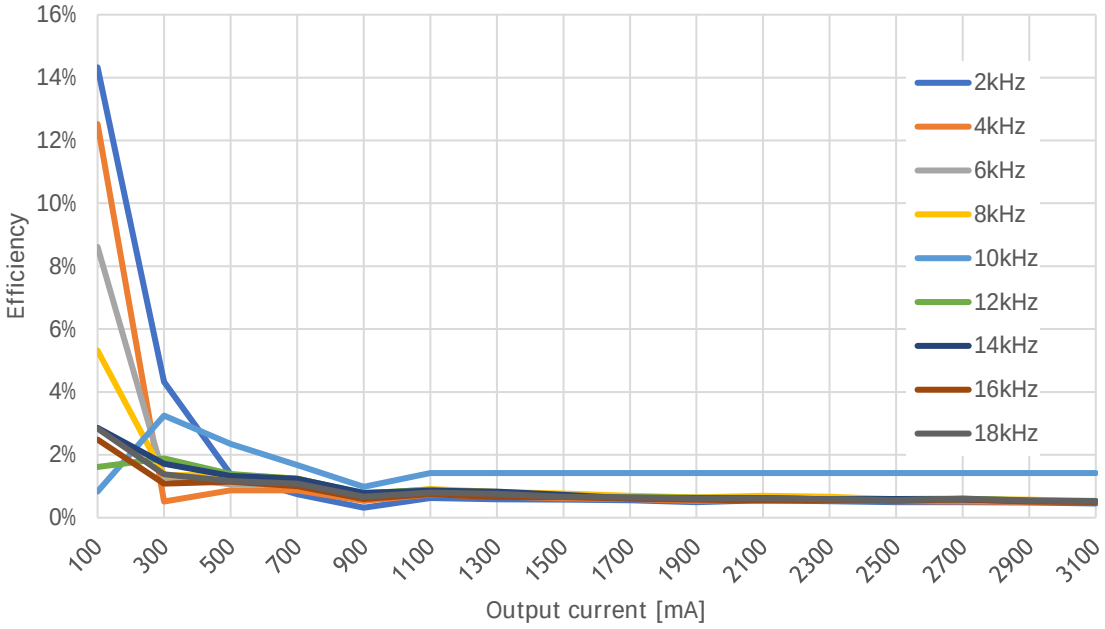

Figure 28: GaN vs Si efficiency difference.

EMPTY PAGE

Chapter 8

Experimental results

Following the simulations developed on Simulink, the same LED lighting system was constructed and tested in a laboratorial environment, as shown in Figure 29. The control part of the buck converter, as well as the acquisition of data was developed using DSpace hardware. The interface between hardware and the user, shown in Figure 30, was implemented using ControlDesk software. Regarding the switching devices, an IGBT SK integrated intelligent Power PACK 3-phase bridge SKiiP 132 GD power module (for the Si devices) and the GS66508B E-mode GaN transistor (for the GaN devices) were adopted in the experiments. Note that, for both cases, the switching devices were accompanied by a driver, which means that only a TTL control signal was necessary.

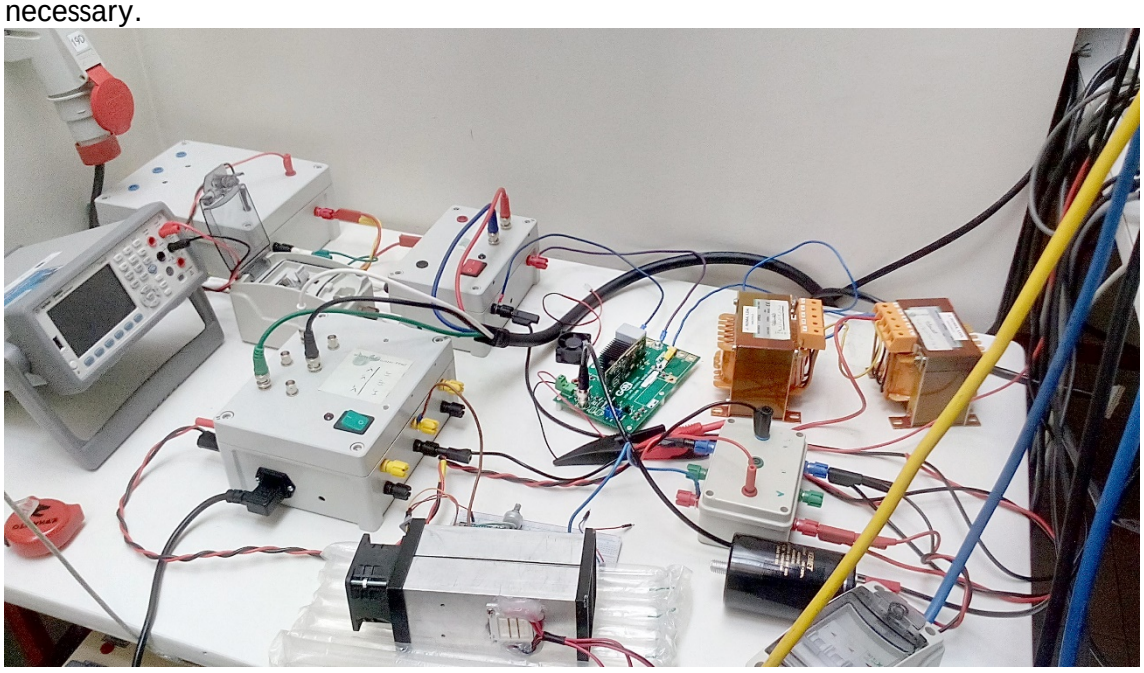

Figure 29: Experimental setup.

The voltage source used consisted on a 3-phase autotransformer, connected to a 3-phase rectifier. In other to smooth the rectifier output voltage, a 3.3mF smoothing capacitor was used. The autotransformer was regulated as to obtain approximately 50 V output, at no-load situation. To protect the circuit against faults, a 6 A slow-burn

fuse was connected between the buck converter and the ground of the voltage source. A circuit breaker was also used between the autotransformer and the grid. The LED was mounted in a heatsink with a 12 W PWM speed-controlled cooling fan. The measurement of current was performed using non-contact current probes, and the voltage was measured resorting to galvanically-isolated voltage probes.

The buck converter output was smoothed using a 400 V 2.2 mF electrolytic capacitor. In order to obtain a 5 mH inductor, two 10 mH inductors were connected in parallel.

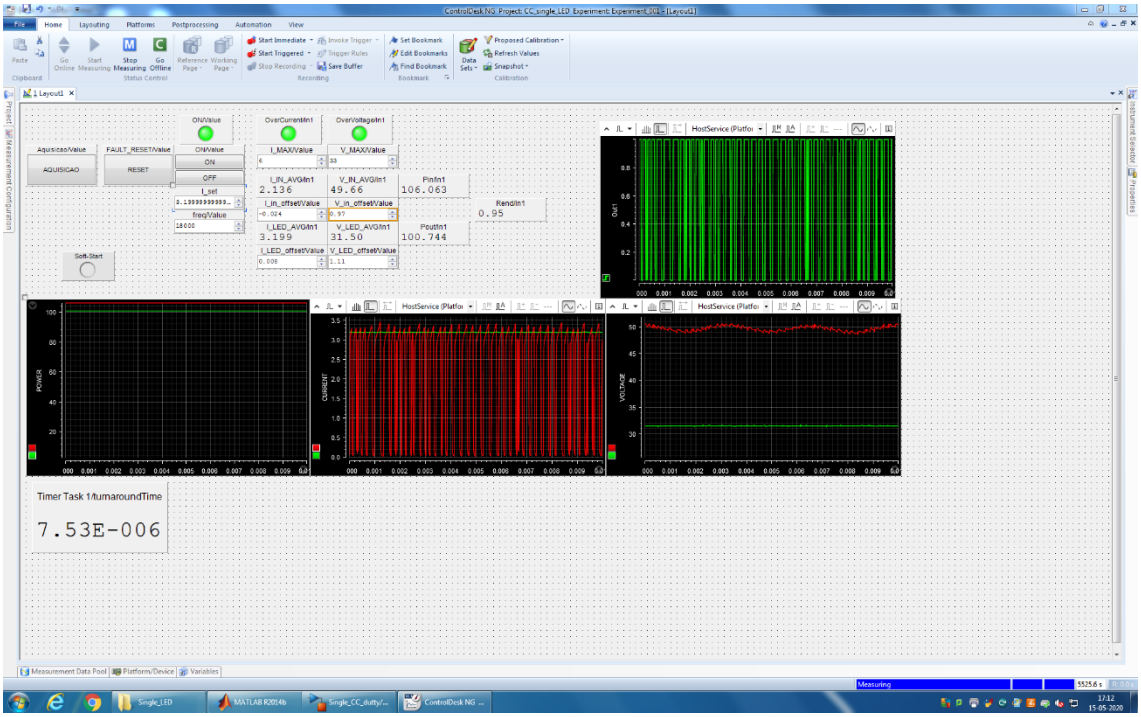

Figure 30: Graphical interface developed in ControlDesk platform.

The graphical interface was used to set the reference of the converter output current, maximum shut-down input current and output voltage level, PWM frequency, and probes offset. The interface was also used to display and monitor, in real time, the waveforms of the current, voltage, and power, at both the input and output. The ON/OFF and protection RESET commands were also controlled through the graphical interface.

The experiments were performed after a warm-up time, allowing all the system to reach a full steady-state condition. The temperature of the LED heatsink was maintained below 40 ºC.

Table 7 shows the efficiency levels of the buck converter based on Si devices, for each frequency and current level, measured in each experimental scenario. Figure 31 depicts the data provided in Table 7, resorting to a graphical representation.

Table 7: Experimental efficiency of the buck converter based on Si devices.

I\f	2kHz	4kHz	6kHz	8kHz	10kHz	12kHz	14kHz	16kHz	18kHz
100	80,81%	67,74%	70,72%	77,39%	66,57%	79,64%	75,10%	75,57%	76,75%
300	87,95%	85,54%	86,76%	90,16%	84,55%	91,43%	88,27%	88,38%	89,49%
500	91,73%	90,27%	91,09%	93,04%	88,46%	93,63%	91,84%	92,14%	92,17%
700	93,78%	92,42%	92,41%	93,51%	90,57%	94,88%	93,55%	93,48%	93,99%
900	94,14%	93,32%	93,63%	95,11%	91,62%	95,67%	94,45%	94,80%	94,86%
1100	95,13%	94,06%	94,83%	94,94%	92,39%	95,75%	95,35%	95,48%	95,12%
1300	95,19%	94,97%	95,24%	95,79%	91,84%	95,46%	96,09%	95,64%	95,08%
1500	94,76%	95,10%	94,58%	95,79%	92,88%	96,21%	95,54%	96,21%	95,65%
1700	95,18%	95,03%	94,98%	96,29%	93,06%	96,07%	95,24%	97,07%	95,28%
1900	95,96%	95,48%	94,80%	96,08%	91,76%	95,10%	95,98%	96,01%	95,64%
2100	95,58%	95,43%	95,63%	95,94%	92,91%	96,03%	95,90%	95,94%	95,84%
2300	95,53%	95,49%	95,79%	95,88%	92,79%	95,96%	95,87%	96,09%	95,93%
2500	95,47%	95,50%	95,87%	95,88%	93,06%	95,86%	95,61%	96,03%	96,59%
2700	94,97%	95,45%	95,68%	96,28%	93,05%	96,61%	95,50%	95,42%	95,72%
2900	96,15%	95,44%	95,91%	95,78%	92,87%	96,14%	95,74%	95,73%	96,15%
3100	95,85%	95,90%	96,21%	95,73%	92,95%	95,86%	95,91%	96,20%	96,22%

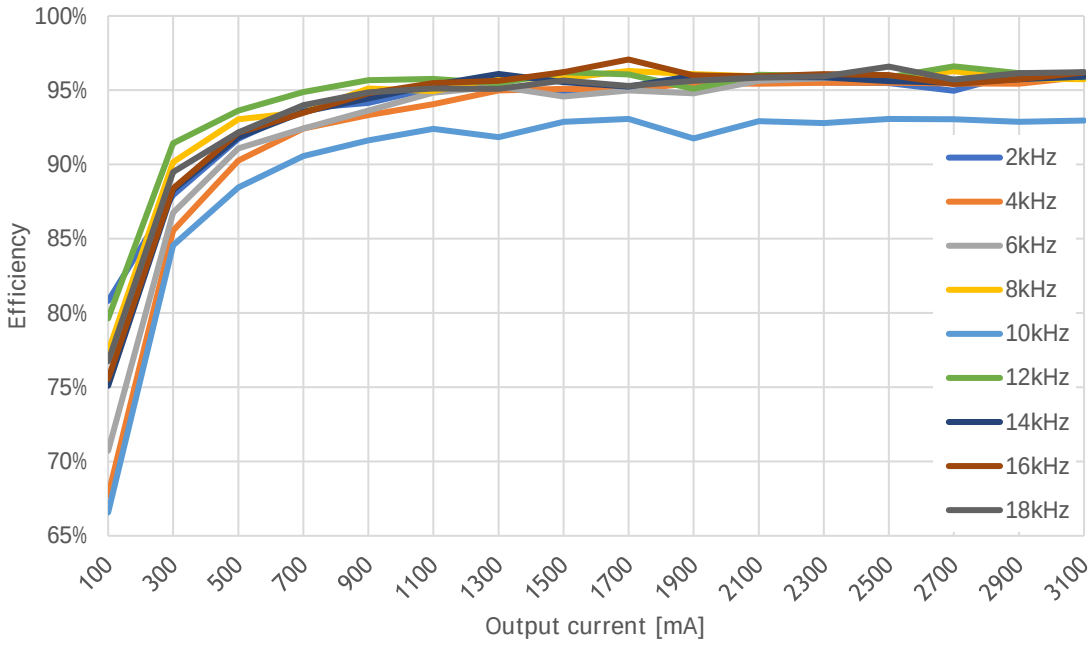

Figure 31: Experimental efficiency of the buck converter based on Si devices.

Table 8 shows the efficiency levels of the buck converter based on GaN devices, for each frequency and current level, measured in each experimental scenario. Figure 32 depicts the data provided in Table 8, resorting to a graphical representation.

Table 8: Experimental efficiency of the buck converter based on GaN devices.

I\f	2kHz	4kHz	6kHz	8kHz	10kHz	12kHz	14kHz	16kHz	18kHz
100	71,89%	71,97%	74,35%	79,09%	78,61%	83,10%	78,57%	83,23%	82,76%
300	88,96%	89,27%	90,26%	92,54%	89,82%	93,40%	92,20%	94,56%	93,93%
500	93,33%	93,50%	94,16%	95,16%	93,64%	95,87%	95,53%	96,34%	96,44%
700	95,23%	95,23%	95,83%	96,50%	95,44%	97,19%	97,25%	97,27%	96,98%
900	96,35%	96,25%	96,75%	97,25%	96,35%	97,72%	97,05%	98,29%	97,35%
1100	96,81%	96,80%	97,17%	97,58%	97,11%	98,19%	97,36%	97,99%	97,54%
1300	97,00%	97,21%	97,30%	97,89%	97,12%	98,12%	97,75%	98,14%	97,44%
1500	97,45%	97,32%	97,59%	97,91%	97,50%	98,23%	98,07%	97,71%	98,32%
1700	97,55%	97,64%	97,90%	98,07%	97,62%	98,19%	97,89%	97,88%	97,97%
1900	97,70%	97,67%	97,70%	98,14%	97,79%	98,39%	97,84%	98,26%	98,17%
2100	97,80%	97,50%	97,85%	98,24%	97,88%	98,27%	97,74%	97,45%	97,74%
2300	97,83%	97,74%	97,87%	98,08%	97,77%	98,14%	97,95%	97,81%	98,23%
2500	97,79%	97,77%	97,83%	98,14%	97,83%	98,11%	97,49%	97,56%	97,95%
2700	97,83%	97,79%	97,79%	98,05%	97,41%	97,93%	97,71%	97,87%	97,74%
2900	97,48%	97,76%	97,78%	98,05%	97,84%	98,11%	97,49%	97,74%	97,91%
3100	97,76%	97,73%	97,79%	98,02%	97,80%	98,03%	97,63%	97,18%	97,71%

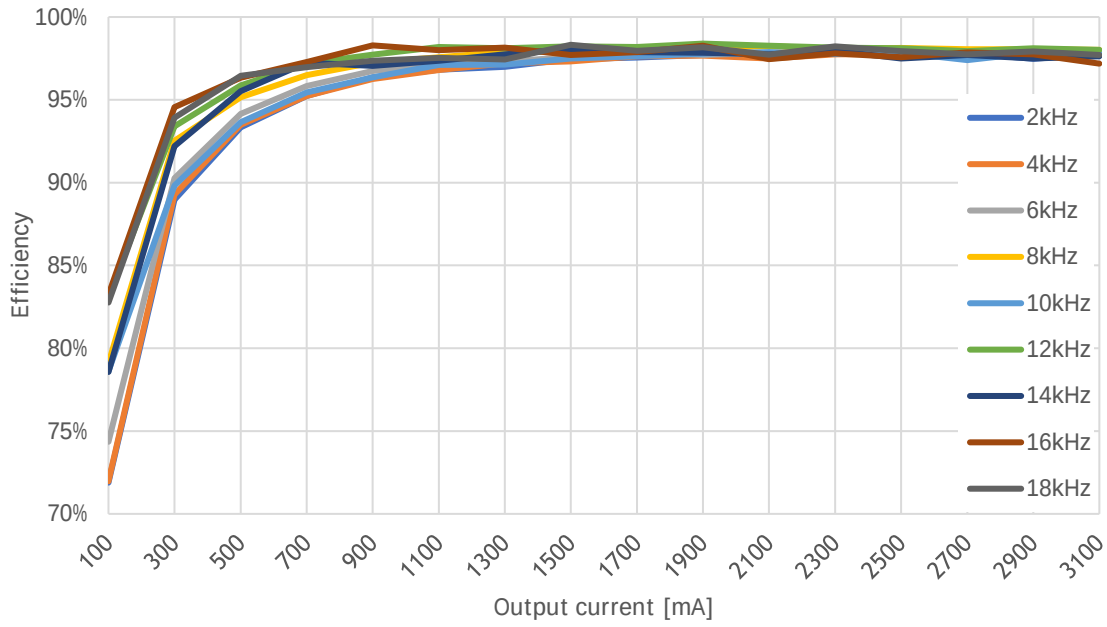

Figure 32: Experimental efficiency of the buck converter based on GaN devices.

To better evaluate the difference between the Si and the GaN technologies in terms of performance, the difference between the efficiency of both systems was computed. The results of such exercise are represented inTable 9: GaN vs Si efficiency difference. Table 9 and Figure 33.

Table 9: GaN vs Si efficiency difference.

I\f	2kHz	4kHz	6kHz	8kHz	10kHz	12kHz	14kHz	16kHz	18kHz
100	1,07%	4,23%	3,63%	1,70%	2,04%	3,46%	3,47%	7,66%	6,02%
300	1,02%	3,73%	3,50%	2,38%	5,26%	1,97%	3,92%	6,18%	4,44%
500	1,60%	3,23%	3,06%	2,11%	5,18%	2,23%	3,69%	4,19%	4,28%
700	1,45%	2,80%	3,41%	2,99%	4,87%	2,31%	3,70%	3,80%	2,99%
900	2,21%	2,93%	3,12%	2,14%	4,73%	2,05%	2,60%	3,49%	2,49%
1100	1,69%	2,74%	2,34%	2,64%	4,72%	2,43%	2,02%	2,51%	2,42%
1300	1,80%	2,24%	2,06%	2,10%	5,28%	2,66%	1,66%	2,51%	2,36%
1500	2,69%	2,23%	3,01%	2,12%	4,62%	2,03%	2,53%	1,51%	2,67%
1700	2,37%	2,61%	2,92%	1,78%	4,57%	2,12%	2,65%	0,82%	2,68%
1900	1,74%	2,19%	2,90%	2,06%	6,03%	3,30%	1,86%	2,26%	2,53%
2100	2,22%	2,08%	2,22%	2,30%	4,97%	2,24%	1,84%	1,51%	1,90%
2300	2,30%	2,25%	2,07%	2,20%	4,98%	2,19%	2,08%	1,72%	2,30%
2500	2,31%	2,27%	1,96%	2,26%	4,77%	2,24%	1,88%	1,54%	1,36%
2700	2,86%	2,33%	2,10%	1,77%	4,36%	1,33%	2,22%	2,45%	2,02%
2900	1,32%	2,32%	1,87%	2,27%	4,97%	1,96%	1,75%	2,01%	1,76%
3100	1,91%	1,83%	1,58%	2,29%	4,84%	2,17%	1,72%	0,98%	1,48%

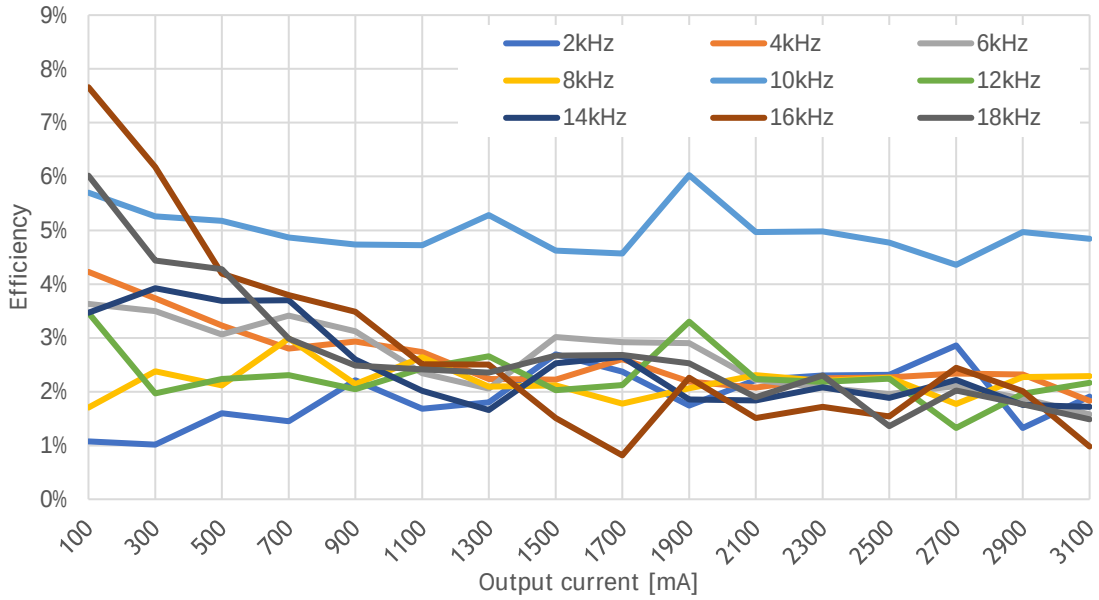

Figure 33: GaN vs Si efficiency difference.

EMPTY PAGE

Chapter 9

RGB LED Driver

RGB LED lighting systems is another interesting application of WBGS within the domain of LED lighting, since a fast-, high-power switching device technology would be profitable for the total efficiency of the lighting system and the improvement of colour rendering. The proposed high-frequency RGB LED driver is used to power a Red, a Green and a Blue string, being each of those strings composed of 8 LEDs connected in parallel.

The controller for the proposed RGB driver, depicted in Figure 34 is based on the controller adopted for the single-channel LED lighting system, detailed in chapter 6. In this controller, a hysteresis control method was included, in order to individually control each one of the colour channels.

The simulations were developed using GaN transistors, considering the parameters defined in chapter 6, and then using Si MOSFETs, considering the parameters expressed in Table 10.

Table 10: Si MOSFET parameters.

Symbol	Parameter	Value	Unit
$R_{ds(on)}$	Drain-source ON resistance (I_{ds} = 6 A, V_{gs} = 10 V)	0.044	Ω
V_{th}	Gate-source threshold voltage	1.7	V
T_{amb}	Environment temperature	25	ºC
C_{iss}	Input capacitance	1960	pF
C_{rss}	Reverse transfer capacitance	40	pF
C_{oss}	Output capacitance	250	pF

The same MOSFETs were used in the commutation of each colour channel, for both GaN and Si simulations.

For each of the two semiconductor technologies, simulations employ a time step of 1 µs, with a duration of 1 s. The main PWM frequency was set to 500 kHz, while the hysteresis control update frequency, related to the period of time assigned to each colour channel, was set to 10 kHz.

Simulations show an efficiency of around 64,62 % for the Si-based controller, while the GaN-based controller achieves an efficiency of around 69,19 %. Therefore, the GaN-based RGB LED driver brings an efficiency improvement of 4,57 %. This efficiency difference can be linked to the influence of the parasitic capacitances in the switching losses, as the frequency increases. At the switching frequency range under consideration in this study, the lower parasitic capacitances of GaN translate into a higher slew rate and, consequently, a shorter period in the ohmic region.

Chapter 10

Conclusions and suggestions for future work

10.1 Conclusions

Based on the data obtained from the simulations, it is possible to observe that, as the output current increases, so does the efficiency, for both Si and GaN technologies. The logarithmic incremental trend of the efficiency is expected because, at low output power, the losses in the inductor and switching devices represent the major part of the input power. Thus, the efficiency suffers a noticeable depreciation for low output power, regardless of the selected semiconductor technology. Also, the effect of the switching frequency observed on the efficiency is negligible, for both technologies. Such behaviour might be explained by the relatively short range of switching frequencies adopted in the study, which translates into an almost null impact on the switching devices and a small impact on the inductor sizing.

From the simulation results compiled in Table 6 and Figure 27, it is perceived that the GaN-based LED drivers are more efficient than the Si-based ones, for every frequency and output current level. Apart the scenarios of very low power, where the measurements may be accompanied by some error, the GaN transistors demonstrate improvements in efficiency within the [0,5 2] % range, when compared to the Si-based LED driver solution.

Referring to the data obtained in the experimental tests, it is concluded that the GaN transistors are more efficient, regardless of the tested frequencies and output currents. The difference in efficiency becomes slightly more prominent at output currents lower than 1100 mA. It is also possible to see a slight deviation from the values obtained from the simulation. This deviation between simulation and experimental results can be related to the introduction of parasitic inductances and capacitances inherent to the experimental setup but, more importantly, due to the fact that some parameters used in the simulations, such as the parasitic capacitances and driver dead-time, were selected based on worst case scenario values, resulting in slightly higher power losses and a marginally smaller efficiency in the simulations.

To complement the efficiency analysis, a simple evaluation of the price and volume of the components was also developed. for the exact same DC-DC converter topology and output power level, taking in consideration the frequency limitations of each system and choosing available of-the-shelf components. Data was compiled in Table 11.

Table 11: Si- vs GaN-based LED driver cost and volume.

		REFERENCE	PRICE [€]	VOLUME [mm^3]
Si	**Switching device**	IRGP4062DPBF	5,58	1636,78
	Driver	IR2104	1,46	35
	Inductor	AIUR-04-103J	0,43	2531,2
		TOTAL:	7,47	4202,98
GaN	**Switching device**	GS66508B	34,2	67,59
	Driver	ADuM4121	5,04	121,84
	Inductor	DENO-25-0001	4,1	230
		TOTAL:	43,34	419,43

GaN transistors are not only more efficient, but also enable the selection of smaller components, making the converter more than 10 times smaller. The drawback for this is their higher cost, around 6 times more expensive than the Si-based converter.

10.2 Suggestions for future work

Considering the acquisition cost of the switching devices and the required components, the use of WBGS in power converters is a feasible option for high-power applications, for applications where high-frequency commutation is used in order to obtain lower output ripple, or in applications where higher frequencies allow the design of power electronic converters with smaller passive components and, therefore, a smaller product. If the higher penetration of WBGS and the large-scale production cuts prices down, the WBGS will become a very attractive option to replace SiS. For LED lighting applications, WBGS are, therefore, an interesting option for high-power lighting applications, like offices or factory lighting, or even public street lighting.

Also, in order to accurately test high-frequency switching systems based on GaN, a dedicated controller or fast acquisition ADC would enhance the quality of the

results, so that it would be possible to test the GaN transistors at frequencies higher than 1 MHz, a region of operation suitable to fully exploit the advantages of GaN in terms of lower parasitic capacitances.

Finally, a careful evaluation of the temperature and power dissipation could provide information deemed useful to evaluate the possibility of developing a lighting system with smaller footprint.

EMPTY PAGE

References

[1] Enerdata, "Global Energy Statistical Yearbook 2019" 2019. [Online]. Available: https://yearbook.enerdata.net/electricity/electricity-domestic-consumption-data.html. [Accessed 27 February 2020].

[2] J. Zhong, Q. Qi, H. He, H. He, T. Ding, and J. He, "Study on Characteristics of Slow-front Overvoltage of ±1100 kV UHVDC Transmission Lines," *The Journal of Engineering,* vol. 2019, no. 16, pp. 1726-1729, 2018.

[3] G. Falahi, "Design, Modeling and Control of Modular Multilevel Converter based HVDC Systems", Raleigh, North Carolina: Dissertation for the degree of Doctor of Philosophy in Electrical Engineering, 2015.

[4] Eurostat, "Energy consumption in households by type of end-use". [Online]. Available: https://ec.europa.eu/eurostat/statistics-explained/index.php/Energy_consumption_in_households#Energy_consumption_in_households_by_type_of_end-use. [Accessed 27 February 2020].

[5] H. Kakigano, M. Nomura, and T. Ise, "Loss Evaluation of DC Distribution for Residential Houses Compared with AC System," in *The 2010 International Power Electronics Conference - ECCE ASIA -*, Sapporo, 2010, pp. 480-486.

[6] K. Techakittiroj, S. Patumtaewapibal, V. Wongpaibool, and W. Threevithayanon, "Roadmap for Implementation of DC System in Future Houses," in *2008 13th International Conference on Harmonics and Quality of Power*, Wollongong, NSW, Australia, 2008, pp. 1-5.

[7] J. D. Irwin, The Industrial Electronics Handbook, 2000 Corporate Blvd., N.W, Boca Raton, Florida 33431: CRC press in cooperation with IEEE press, 1997.

[8] Energy Office of Energy Efficiency & Renewable Energy, "How Energy-Efficient Light Bulbs Compare with Traditional Incandescents," Office of Energy Efficiency & Renewable Energy, [Online]. Available: https://www.energy.gov/energysaver/save-electricity-and-fuel/lighting-choices-save-you-money/how-energy-efficient-light. [Accessed 19 February 2020].

[9] Rensselaer Polytechnic Institute, "Lighting Answers-How are LEDs affected by heat?," 2003. [Online]. Available: https://www.lrc.rpi.edu/programs/nlpip/lightinganswers/led/heat.asp. [Accessed 20 February 2020].

[10] R. v. Roy, *Minimizing Light Flicker in LED Lighting Applications*, Taiwan: Richtek Technology Corporation, July 2014.

[11] P. R. Boyce, *Human Factors in Lighting - Third Edition*, 6000 Broken Sound Parkway NW, Suite 300 Boca Raton, FL 33487-2742: CRC Press Taylor & Francis Group, 2014.

[12] L. Németh, 25 June 2013. [Online]. Available: https://commons.wikimedia.org/wiki/File:RGB_color_wheel_360.svg. [Accessed 27 February 2020].

[13] J. L. Hudgins, G. S. Simin, E. Santi, and M. A. Khan, "An Assessment of Wide Bandgap Semiconductors for Power Devices," *IEEE Transactions On Power Electronics,* vol. 18, no. 3, pp. 907-914, 2003.

[14] S. Pearton, C. Abernathy, M. Overberg, G. Thaler, A. Onstine, B. Gila, F. Ren, B. Lou, and J. Kim, "New applications advisable for gallium nitride," *Materials Today*, 2002, pp. 24-31.

[15] "Diemat, Inc," [Online]. Available: http://diemat.com/docs/products/thermals/thermal_properties.php. [Accessed 21 Febuary 2020].

[16] Mouser ELETRONICS, Inc., [Online]. Available: https://pt.mouser.com/Search/Refine?Ntk=P_MarCom&Ntt=166756581. [Accessed Julho 2019].

[17] "Product Brief-IHM, IHV Modules & PrimePACK™," Infineon Technologies AG, 85579 Neubiberg, Germany, 2016.

[18] M. Danilovic, Z. Chen, R. R. Wang, F. Luo, D. Boroyevich, and P. Mattavelli, "Evaluation of the switching characteristics of a gallium-nitride transistor," *IEEE Energy Conversion Congress and Exposition,* pp. 2581-2688, 2011.

[19] B. Ozpineci and L. M. Tolbert, "Comparison of Wide-Bandgap Semiconductors for Power Electronic Applications", Oak Ridge, Tennessee, USA: U.S. Department of Energy, 2003.

[20] S. Azzopardi, A. Kawamura, and H. Iwamoto, "Soft-switching performances of 1200V new punch-through IGBT using local lifetime control at high temperature," in *2001 IEEE 32nd Annual Power Electronics Specialists Conference,* vol. 2, pp. 606-611, 2001.

[21] R. L. Greenwell, B. M. McCue, L. M. Tolbert, B. J. Blalock, and S. K. Islam, "High-Temperature SOI-Based Gate Driver IC for WBG Power Switches," in *Twenty-Eighth Annual IEEE Applied Power Electronics Conference and Exposition (APEC)*, Long Beach, CA, USA, 2013, pp. 1768-1775.

[22] S. Davis, "Power Management Chapter 11: Wide Bandgap Semiconductors," Power Electronics, May 2018. [Online]. Available: https://www.powerelectronics.com/technologies/power-management/article/21864166/power-management-chapter-11-wide-bandgap-semiconductors. [Accessed 26 Febuary 2020].

[23] IGBT & SiC Gate Driver Fundamentals, Texas Instruments, Post Office Box 655303, Dallas, Texas 75265, 2019.

[24] H. Shibata, Y. Waseda, H. Ohta, K. Kiyomi, K. Shimoyama, K. Fujito, H. Nagaoka, Y. Kagamitani and R. S. a. T. Fukuda, “High Thermal Conductivity of Gallium Nitride (GaN) Crystals Grown by HVPE Process,” Materials Transactions, vol. 48, no. 10, pp. 2782 -2786, 2007.